FISEVIER

Contents lists available at ScienceDirect

Journal of Computational Physics

www.elsevier.com/locate/jcp



A new primal-dual weak Galerkin method for elliptic interface problems with low regularity assumptions



Waixiang Cao ^{a,1}, Chunmei Wang ^{b,*,2}, Junping Wang ^{c,3}

- ^a School of Mathematical Sciences, Beijing Normal University, Beijing 100875, China
- ^b Department of Mathematics, University of Florida, Gainesville, FL 32611, USA
- ^c Division of Mathematical Sciences, National Science Foundation, Alexandria, VA 22314, USA

ARTICLE INFO

Article history:

Received 23 October 2020 Received in revised form 17 July 2022 Accepted 10 August 2022 Available online 28 August 2022

Keywords:

Primal-dual weak Galerkin PDWG Finite element methods Elliptic interface problems Low regularity Polygonal or polyhedral partition

ABSTRACT

This article introduces a new primal-dual weak Galerkin (PDWG) finite element method for second order elliptic interface problems with ultra-low regularity assumptions on the exact solution and the interface and boundary data. It is proved that the PDWG method is stable and accurate with optimal order of error estimates in discrete and Sobolev norms. In particular, the error estimates are derived under the low regularity assumption of $u \in H^{\delta}(\Omega)$ for $\delta > \frac{1}{2}$ for the exact solution u. Extensive numerical experiments are conducted to provide numerical solutions that verify the efficiency and accuracy of the new PDWG method.

© 2022 Elsevier Inc. All rights reserved.

1. Introduction

In this paper we are concerned with the development of a new primal-dual weak Galerkin (PDWG) finite element method for second order elliptic interface problems with low regularity assumptions on the exact solution and the interface and boundary data. To this end, let N and M be two positive integers and $\Omega \subset \mathbb{R}^d (d=2,3)$ is an open bounded domain with piecewise smooth Lipschitz boundary $\partial \Omega$. The domain Ω is partitioned into a set of subdomains $\{\Omega_i\}_{i=1}^N$ with piecewise smooth Lipschitz boundary $\partial \Omega_i$ for $i=1,\cdots,N$; $\Gamma=\bigcup_{i=1}^N\partial \Omega_i\setminus\partial \Omega$ is the interface between the subdomains in the sense that

$$\Gamma = \bigcup_{m=1}^{M} \Gamma_m,$$

where there exist $i, j \in \{1, \dots, N\}$ such that $\Gamma_m = \partial \Omega_i \cap \partial \Omega_j$ for $m = 1, \dots, M$. The elliptic interface problem seeks an unknown function u satisfying

E-mail addresses: caowx@bnu.edu.cn (W. Cao), chunmei.wang@ufl.edu (C. Wang), jwang@nsf.gov (J. Wang).

^{*} Corresponding author.

The research of Waixiang Cao was partially supported by NSFC grant No. 11871106.

² The research of Chunmei Wang was partially supported by National Science Foundation Award DMS-2136380.

³ The research of Junping Wang was supported in part by the NSF IR/D program, while working at National Science Foundation. However, any opinion, finding, and conclusions or recommendations expressed in this material are those of the author and do not necessarily reflect the views of the National Science Foundation.

$$-\nabla \cdot (a_i(x)\nabla u_i) + \nabla \cdot (\mathbf{b}_i(x)u_i) + c_i u_i = f_i, \qquad \text{in } \Omega_i, i = 1, \dots, N, \tag{1.1}$$

$$u_i = g_i,$$
 on $\partial \Omega_i \cap \partial \Omega, i = 1, \dots, N,$ (1.2)

$$\llbracket u \rrbracket_{\Gamma_m} = \phi_m,$$
 on $\Gamma_m, m = 1, \dots, M,$ (1.3)

$$[\![(a\nabla u - \mathbf{b}u) \cdot \mathbf{n}]\!]_{\Gamma_m} = \psi_m, \qquad \text{on} \quad \Gamma_m, m = 1, \dots, M,$$
(1.4)

where $u_i = u|_{\Omega_i}$, $a_i = a|_{\Omega_i}$, $\mathbf{b}_i = \mathbf{b}|_{\Omega_i}$, $c_i = c|_{\Omega_i}$, and $[\![(a\nabla u - \mathbf{b}u) \cdot \mathbf{n}]\!]_{\Gamma_m} = (a_i\nabla u_i - \mathbf{b}_iu_i) \cdot \mathbf{n}_i + (a_j\nabla u_j - \mathbf{b}_ju_j) \cdot \mathbf{n}_j$ with \mathbf{n}_i and \mathbf{n}_j being the unit outward normal directions to $\partial\Omega_i \cap \Gamma_m$ and $\partial\Omega_j \cap \Gamma_m$, and $[\![u]\!]_{\Gamma_m} = u_i|_{\Gamma_m} - u_j|_{\Gamma_m}$. Assume the elliptic coefficients a, \mathbf{b} and c are piecewise smooth with respect to the partition $\Omega = \bigcup_{i=1}^N \Omega_i$. We further assume that a(x) is symmetric and positive definite matrices uniformly in Ω .

Elliptic interface problems arise in many applications of mathematical modeling and simulation of practical problems in science and engineering. These applications include computational electromagnetic [18,23,54,53], fluid mechanics [30], materials science [24,28], and biological science [52,14,7], to mention just a few. The physical solution to interface problems often possesses discontinuity and/or non-smoothness across the interfaces so that the standard numerical methods will not work at their full capacity. To address this challenge, many finite element methods (FEMs) [38,4,9,12,42] and finite difference methods based on Cartesian grids [41,40,31,33,1] have been developed for effective solving of the elliptic interface problem in the last several decades. In the classical FEMs, unstructured partitions were employed to deal with the irregularity of the domain geometry, particularly around the interface and domain boundary. The interface-fitted FEMs are based on proper formulations of the interface problem combined with finite element partitions that align well with the interface. The penalty methods or Lagrangian multiplier approaches were developed in [16.6] by imposing the interface condition in the weak formulation. Incorporating the interface conditions into the numerical formulation has the potential of not only increasing the accuracy of the approximate solutions near the interface, but also the flexibility of allowing the use of computational grids that do not align with the physical interfaces. The discontinuous Galerkin (DG) methods [11,17,21,29] were developed by using Galerkin projections and properly defined numerical fluxes to enforce the interface conditions in a weak sense. Weak Galerkin (WG) FEMs have been developed in [37,38] by using discrete weak differential operators in the usual variational form of the elliptic interface problem together with a treatment of the interface condition via the boundary unknowns associated with the weak finite element approximations. The embedded or immersed FEMs [12,19,25,45,20,26, 35,27,47,48] were devised to allow the interface to cut through finite elements for problems with moving interfaces and complex topology. Consequently, structured Cartesian meshes could be used to avoid the time-consuming mesh generation process in the immersed FEMs. Recently, a Hybrid High-Order (HHO) method on unfitted meshes was designed and analyzed in [5] for elliptic interface problems by means of a consistent penalty method in which the curved interface is allowed to cut through the mesh cells in a general fashion.

Numerical methods in the context of finite differences for the elliptic interface problem include the ghost fluid method [13], maximum principle preserving and explicit jump immersed interface method (IIM) [32,46,3,33], coupling interface method [10], piecewise-polynomial interface method [8], and matched interface and boundary (MIB) method [54,55,50]. For problems with non-smooth interfaces, some second order finite difference schemes have been devised in the context of the MIB framework in 2D and 3D [51,52,47,48]. Other algorithms based on various mathematical techniques for the elliptic interface problem include the integral equation method [36,49], the finite volume method [39], and the virtual node method [2,22].

Even though successes have been achieved in the endeavor of solving elliptic interface problems, challenges remain in the search of new and efficient numerical algorithms for problems with very complicated interface geometries, and for problems with low-regularity solutions. The low-regularity of the solution is often caused by the geometric singularities of the interfaces and/or the non-smoothness of the interface data [37,26].

The goal of this paper is to develop a new numerical method for the elliptic interface problem (1.1)-(1.4) which is applicable to solutions with low-regularity assumptions. This new method is devised by coupling a weak formulation of (1.1)-(1.4) that is derivative-free on the exact solution u with its dual equation, yielding a new primal-dual weak Galerkin finite element method (PDWG). Compared with the WG methods [37,38], the proposed PDWG results in a symmetric formulation for a non-symmetric interface problem. More importantly, the new PDWG method is applicable to the model problem (1.1)-(1.4) with rough boundary and interface data on g_i , ϕ_m , and ψ_m . The new method thus provides an efficient numerical algorithm for elliptic interface problems under low regularity assumptions for the exact solution.

The paper is organized as follows. In Section 2, we derive a weak formulation for the elliptic interface problem (1.1)-(1.4) that is derivative-free on the solution variable. In Section 3, we briefly review the weak differential operators and their discrete analogies. In Section 4, we describe the PDWG method for the model problem (1.1) based on the weak formulation (2.1) and its dual. In Section 5, we establish the solution existence, uniqueness, and stability. In Section 6, we provide an error equation for the PDWG solutions. In Section 7, we derive some error estimates based on various regularity assumptions on the exact solution. Finally, in Section 8 we report a couple of numerical results to illustrated and verify our convergence theory.

2. Preliminaries and notations

We follow the standard notations for Sobolev spaces and norms defined on a given open and bounded domain $D \subset \mathbb{R}^d$ with Lipschitz continuous boundary. As such, $\|\cdot\|_{s,D}$ and $|\cdot|_{s,D}$ are used to denote the norm and seminorm in the Sobolev space $H^s(D)$ for any $s \geq 0$. The inner product in $H^s(D)$ is denoted by $(\cdot, \cdot)_{s,D}$ for $s \geq 0$. The space $H^0(D)$ coincides with $L^2(D)$ (i.e., the space of square integrable functions), for which the norm and the inner product are denoted as $\|\cdot\|_D$ and $(\cdot, \cdot)_D$. The space $H^s(D)$ for s < 0 is defined as the dual of $H_0^{-s}(D)$ [15] through the usual $L^2(D)$ pairing. When $D = \Omega$ or when the domain of integration is clear from the context, we shall drop the subscript D in the norm and the inner product notation.

We introduce the following space

$$V = \left\{ v: \ v \in H^1_0(\Omega) \cap \prod_{i=1}^N H^2(\Omega_i), \ a \nabla v \in H(\mathrm{div}; \Omega) \right\}.$$

For sufficiently smooth boundary and interface data g_i , ϕ_m , and ψ_m , the solution of the elliptic interface problem (1.1)-(1.4) satisfies the following weak formulation:

$$(u, \mathcal{L}(v) - \mathbf{b} \cdot \nabla v + cv) = \phi(v), \qquad \forall v \in V, \tag{2.1}$$

where $\mathcal{L}(v)|_{\Omega_i} = -\nabla \cdot (a_i(x)\nabla v|_{\Omega_i})$ and

$$\phi(v) = (f, v) - \sum_{i=1}^{N} \langle \mathbf{g}_i, a_i \nabla v \cdot \mathbf{n}_i \rangle_{\partial \Omega_i \cap \partial \Omega} - \sum_{m=1}^{M} \langle \phi_m, a_i \nabla v \cdot \mathbf{n}_m \rangle_{\Gamma_m} + \sum_{m=1}^{M} \langle \psi_m, v \rangle_{\Gamma_m}.$$

Here $f|_{\Omega_i}=f_i$, \mathbf{n}_i in the term $\sum_{i=1}^N \langle g_i, a_i \nabla v \cdot \mathbf{n}_i \rangle_{\partial \Omega_i \cap \partial \Omega}$ is the unit outward normal direction to the boundary $\partial \Omega_i \cap \partial \Omega$ for $i=1,\cdots,N$. The unit vector \mathbf{n}_m is normal to the interface Γ_m and has a direction consistent with the interface condition (1.4). The weak form (2.1) can be derived by testing (1.1) against any $v \in V$ followed by twice use of the divergence theorem. For boundary and interface data that are not smooth (e.g., for $\phi_m, \psi_m \in L^2(\Gamma_m)$ and $g_i \in L^2(\partial \Omega_i \cap \partial \Omega)$), the elliptic interface problem may not possess a strong solution satisfying (1.1)-(1.4) in the classical sense, but it may have a solution with low-regularity that satisfies the weak form (2.1).

Definition 2.1. A function $u \in L^2(\Omega)$ is said to be a weak solution of the elliptic interface problem (1.1)-(1.4) if it satisfies (2.1).

The dual or adjoint problem to (2.1) seeks an unknown function $\lambda \in V$ such that

$$(w, \mathcal{L}(\lambda) - \mathbf{b} \cdot \nabla \lambda + c\lambda) = \chi(w), \quad \forall w \in H^{\epsilon}(\Omega),$$
 (2.2)

where χ is a given functional in $H^{\epsilon}(\Omega)$. In the rest of the paper, we assume that the dual or adjoint problem (2.2) has one and only one solution in $H^{2-\epsilon}(\Omega)$ with the following regularity estimate

$$\|\lambda\|_{2-\epsilon} \le C\|\chi\|_{-\epsilon}. \tag{2.3}$$

This regularity assumption implies that when $\chi \equiv 0$, the dual problem (2.2) has only the trivial solution $\lambda \equiv 0$. We point out that the adjoint problem is a regular second order elliptic problem involving no interfaces at all.

The weak variational problem (or primal equation) (2.1) and its dual form (2.2) are seemingly unrelated to each other in the continuous case. However, they are strongly connected and support each other in the context of the weak Galerkin approach for each of them. The rest of the paper will reveal this connection and show how they support each other and jointly provide an efficient numerical method for the elliptic interface problem (1.1)-(1.4).

3. Weak differential operators

The two principal differential operators in the weak formulation (2.1) for the second order elliptic interface problem (1.1) are \mathcal{L} and the gradient operator ∇ . The discrete weak version for \mathcal{L} and ∇ has been introduced in [44,43]. For completeness, we shall briefly review their definition in this section.

Let T be a polygonal or polyhedral domain with boundary ∂T . A weak function on T refers to a triplet $\sigma = \{\sigma_0, \sigma_b, \sigma_n\}$ with $\sigma_0 \in L^2(T)$, $\sigma_b \in L^2(\partial T)$ and $\sigma_n \in L^2(\partial T)$. Here σ_0 and σ_b are used to represent the value of σ in the interior and on the boundary of T and σ_n is reserved for the value of $a\nabla \sigma \cdot \mathbf{n}$ on ∂T . Note that σ_b and σ_n may not necessarily be the trace of σ_0 and $a\nabla \sigma_0 \cdot \mathbf{n}$ on ∂T , respectively. Denote by $\mathcal{W}(T)$ the space of weak functions on T:

$$\mathcal{W}(T) = \{ \sigma = \{ \sigma_0, \sigma_h, \sigma_n \} : \sigma_0 \in L^2(T), \sigma_h \in L^2(\partial T), \sigma_n \in L^2(\partial T) \}. \tag{3.1}$$

The weak action of $\mathcal{L} = -\nabla \cdot (a\nabla)$ on $\sigma \in \mathcal{W}(T)$, denoted by $\mathcal{L}_w \sigma$, is defined as a linear functional on $H^2(T)$ such that

$$(\mathcal{L}_w \sigma, w)_T = (\sigma_0, \mathcal{L}w)_T + \langle \sigma_b, a \nabla w \cdot \mathbf{n} \rangle_{\partial T} - \langle \sigma_n, w \rangle_{\partial T},$$

for all $w \in H^2(T)$.

The weak gradient of $\sigma \in \mathcal{W}(T)$, denoted by $\nabla_w \sigma$, is defined as a linear functional on $[H^1(T)]^d$ such that

$$(\nabla_{\boldsymbol{w}}\boldsymbol{\sigma}, \boldsymbol{\psi})_T = -(\sigma_0, \nabla \cdot \boldsymbol{\psi})_T + \langle \sigma_b, \boldsymbol{\psi} \cdot \mathbf{n} \rangle_{\partial T},$$

for all $\psi \in [H^1(T)]^d$.

Denote by $P_r(T)$ the space of polynomials on T with degree no more than r. A discrete version of $\mathcal{L}_w \sigma$ for $\sigma \in \mathcal{W}(T)$, denoted by $\mathcal{L}_{w,r,T} \sigma$, is defined as the unique polynomial in $P_r(T)$ satisfying

$$(\mathcal{L}_{w,r,T}\sigma, w)_T = (\sigma_0, \mathcal{L}w)_T + \langle \sigma_b, a\nabla w \cdot \mathbf{n} \rangle_{\partial T} - \langle \sigma_n, w \rangle_{\partial T}, \quad \forall w \in P_r(T),$$
(3.2)

which, from the usual integration by parts, gives

$$(\mathcal{L}_{w,T,T}\sigma, w)_T = (\mathcal{L}\sigma_0, w)_T - \langle \sigma_0 - \sigma_b, a\nabla w \cdot \mathbf{n} \rangle_{\partial T} + \langle a\nabla \sigma_0 \cdot \mathbf{n} - \sigma_b, w \rangle_{\partial T}, \tag{3.3}$$

for all $w \in P_r(T)$, provided that $\sigma_0 \in H^2(T)$.

A discrete version of $\nabla_w \sigma$ for $\sigma \in \mathcal{W}(T)$, denoted by $\nabla_{w,r,T} \sigma$, is defined as a unique polynomial vector in $[P_r(T)]^d$ satisfying

$$(\nabla_{w,r,T}\sigma, \boldsymbol{\psi})_T = -(\sigma_0, \nabla \cdot \boldsymbol{\psi})_T + (\sigma_b, \boldsymbol{\psi} \cdot \mathbf{n})_{\partial T}, \quad \forall \boldsymbol{\psi} \in [P_r(T)]^d, \tag{3.4}$$

which, from the usual integration by parts, gives

$$(\nabla_{w,r,T}\sigma, \boldsymbol{\psi})_T = (\nabla\sigma_0, \boldsymbol{\psi})_T - \langle \sigma_0 - \sigma_b, \boldsymbol{\psi} \cdot \mathbf{n} \rangle_{\partial T}, \quad \forall \boldsymbol{\psi} \in [P_r(T)]^d, \tag{3.5}$$

provided that $\sigma_0 \in H^1(T)$.

4. Primal-dual weak Galerkin algorithm

Let \mathcal{T}_h be a finite element partition of the domain Ω consisting of polygons or polyhedra that are shape-regular [43]. Assume that the edges/faces of the elements in \mathcal{T}_h align with the interface Γ . The partition \mathcal{T}_h can be grouped into N sets of elements denoted by $\mathcal{T}_h^i = \mathcal{T}_h \cap \Omega_i$, so that each \mathcal{T}_h^i provides a finite element partition for the subdomain Ω_i for $i=1,\cdots,N$. The intersection of the partition \mathcal{T}_h also introduces a finite element partition for the interface Γ , denoted by Γ_h . Denote by \mathcal{E}_h the set of all edges or flat faces in \mathcal{T}_h and $\mathcal{E}_h^0 = \mathcal{E}_h \setminus \partial \Omega$ the set of all interior edges or flat faces. Denote by h_T the meshsize of $T \in \mathcal{T}_h$ and $T \in \mathcal{T}_h$ and $T \in \mathcal{T}_h$ the meshsize for the partition T_h .

For any given integer $k \ge 1$, denote by $W_k(T)$ the local discrete space of the weak functions given by

$$W_k(T) = \{ \{\sigma_0, \sigma_h, \sigma_n\} : \sigma_0 \in P_k(T), \sigma_h \in P_k(e), \sigma_n \in P_{k-1}(e), e \subset \partial T \}.$$

Patching $W_k(T)$ over all the elements $T \in \mathcal{T}_h$ through a common value σ_b on the interior interface \mathcal{E}_h^0 , we arrive at the following weak finite element space W_h :

$$W_h = \{ \{\sigma_0, \sigma_b, \sigma_n\} : \{\sigma_0, \sigma_b, \sigma_n\} |_T \in W_k(T), \forall T \in \mathcal{T}_h \}.$$

Note that σ_n has two values σ_n^L and σ_n^R satisfying $\sigma_n^L + \sigma_n^R = 0$ on each interior interface $e = \partial T_L \cap \partial T_R \in \mathcal{E}_h^0$ as seen from the two elements T_L and T_R . Denote by W_h^0 the subspace of W_h with homogeneous boundary values; i.e.,

$$W_h^0 = \{ \{\sigma_0, \sigma_b, \sigma_n\} \in W_h : \sigma_b|_{\partial\Omega} = 0 \}.$$

Denote by M_h the finite element space consisting of piecewise polynomials of degree k-1; i.e.,

$$M_h = \{w : w | T \in P_{k-1}(T), \forall T \in T_h\}.$$

For simplicity of notation and without confusion, for any $\sigma \in W_h$, denote by $\mathcal{L}_w \sigma$ and $\nabla_w \sigma$ the discrete weak actions $\mathcal{L}_{w,k-1,T}\sigma$ and $\nabla_{w,k-1,T}\sigma$ computed by using (3.2) and (3.4) on each element T; i.e.,

$$(\mathcal{L}_w \sigma)|_T = \mathcal{L}_{w,k-1,T}(\sigma|_T), \qquad \sigma \in W_h,$$

$$(\nabla_w \sigma)|_T = \nabla_{w,k-1,T}(\sigma|_T), \qquad \sigma \in W_h.$$

For any σ , $\lambda \in W_h$ and $u \in M_h$, we introduce the following bilinear forms

$$s(\sigma,\lambda) = \sum_{T \in \mathcal{T}_h} s_T(\sigma,\lambda),\tag{4.1}$$

$$b(u,\lambda) = \sum_{T \in \mathcal{T}_b} b_T(u,\lambda),\tag{4.2}$$

where

$$s_T(\sigma, \lambda) = h_T^{-3} \langle \sigma_0 - \sigma_b, \lambda_0 - \lambda_b \rangle_{\partial T} + h_T^{-1} \langle a \nabla \sigma_0 \cdot \mathbf{n} - \sigma_n, a \nabla \lambda_0 \cdot \mathbf{n} - \lambda_n \rangle_{\partial T} + \tau(\sigma_0, \lambda_0)_T,$$

$$b_T(u, \lambda) = (u, \mathcal{L}_w \lambda - \mathbf{b} \cdot \nabla_w \lambda + c\lambda_0)_T$$

with $\tau > 0$ being a parameter.

The following is the primal-dual weak Galerkin scheme for the second order elliptic interface problem (1.1) based on the variational formulation (2.1).

Primal-Dual Weak Galerkin Algorithm 4.1. Find $(u_h; \lambda_h) \in M_h \times W_h^0$, such that

$$s(\lambda_h, \sigma) + b(u_h, \sigma) = \phi_h(\sigma), \quad \forall \sigma \in W_h^0,$$
 (4.3)

$$b(w, \lambda_h) = 0, \qquad \forall w \in M_h. \tag{4.4}$$

Here $\phi_h(\sigma) = (f, \sigma_0) - \sum_{i=1}^N \langle g_i, \sigma_n \rangle_{\partial \Omega_i \cap \partial \Omega} - \sum_{m=1}^M \langle \phi_m, \sigma_n \rangle_{\Gamma_m} + \sum_{m=1}^M \langle \psi_m, \sigma_b \rangle_{\Gamma_m}$.

5. Stability analysis

Let Q_0 be the L^2 projection operator onto $P_k(T)$, $k \ge 1$. Analogously, denote by Q_b and Q_n the L^2 projection operators onto $P_k(e)$ and $P_{k-1}(e)$, respectively, for $e \subset \partial T$. For $w \in H^1(\Omega)$, define the L^2 projection $Q_h w \in W_h$ as follows

$$Q_h w|_T = \{Q_0 w, Q_b w, Q_n (a \nabla w \cdot \mathbf{n})\}.$$

The L^2 projection operator onto the finite element space M_h is denoted as \mathcal{Q}_h^{k-1} . For simplicity, we assume the coefficient coefficients a(x), $\mathbf{b}(x)$ and c(x) are piecewise constants with respect to the finite element partition \mathcal{T}_h . The analysis can be extended to piecewise smooth coefficients a(x), $\mathbf{b}(x)$ and c(x) without any difficulty.

Lemma 5.1. [44,43] The operators Q_h and Q_h^{k-1} satisfy the following commutative properties:

$$\mathcal{L}_{w}(Q_{h}w) = \mathcal{Q}_{h}^{k-1}(\mathcal{L}w), \qquad \forall w \in H^{2}(T), \tag{5.1}$$

$$\nabla_{w}(Q_{h}w) = \mathcal{Q}_{h}^{k-1}(\nabla w), \qquad \forall w \in H^{1}(T). \tag{5.2}$$

The stabilizer $s(\cdot, \cdot)$ given in (4.1) naturally induces the following semi-norm in the weak finite element space W_h

$$\|\rho\|_{w} = s(\rho, \rho)^{\frac{1}{2}}, \qquad \rho \in W_{h}.$$
 (5.3)

Lemma 5.2. The semi-norm $\|\cdot\|_{W}$ given in (5.3) defines a norm in the linear space W_{h}^{0} .

Proof. It suffices to verify the positivity property for $\|\cdot\|_w$. Assume $\|\rho\|_w = 0$ for some $\rho \in W_h^0$. It follows that $\rho_0 = 0$ on each element T, $\rho_0 = \rho_h$ and $a \nabla \rho_0 \cdot \mathbf{n} = \rho_h$ on each ∂T . We thus obtain $\rho_0 \in C^0(\Omega)$ and further $\rho_0 \equiv 0$ in Ω . Using $\rho_0 = \rho_h$ and $a\nabla \rho_0 \cdot \mathbf{n} = \rho_n$ on each ∂T gives $\rho_b \equiv 0$, $\rho_n \equiv 0$, and further $\rho \equiv 0$ in Ω . This completes the proof of the lemma. \square

Consider the auxiliary problem of seeking Φ such that

$$\mathcal{L}(\Phi) - \mathbf{b} \cdot \nabla \Phi + c \Phi = \psi, \quad \text{in } \Omega, \tag{5.4}$$

$$\Phi = 0, \qquad \text{on } \partial\Omega, \tag{5.5}$$

where $\psi \in L^2(\Omega)$ is a given function. Assume that the problem (5.4)-(5.5) has a solution $\Phi \in \prod_{i=1}^N H^{1+\gamma}(\Omega_i)$ satisfying

$$\left(\sum_{i=1}^{N} \|\Phi\|_{1+\gamma,\Omega_i}^2\right)^{\frac{1}{2}} \le C\|\psi\|_{\gamma-1},\tag{5.6}$$

with some parameter $\gamma \in (\frac{1}{2}, 1]$.

Lemma 5.3. (inf-sup condition) Under the assumption of (5.6), there exists a constant $\beta > 0$ independent of the meshsize h such that

$$\sup_{0 \neq \sigma \in W_h^0} \frac{b(v, \sigma)}{\|\sigma\|_w} \ge \beta h^{1-\gamma} \|v\|_{1-\gamma}, \qquad \forall v \in M_h.$$

$$(5.7)$$

Proof. Let Φ be the solution of (5.4)-(5.5) satisfying (5.6). By letting $\sigma = Q_h \Phi$, we have from Lemma 5.1 and (5.4) that

$$b(v,\sigma) = \sum_{T \in \mathcal{T}_h} (v, \mathcal{L}_w(Q_h \Phi) - \mathbf{b} \cdot \nabla_w Q_h \Phi + c Q_0 \Phi)_T$$

$$= \sum_{T \in \mathcal{T}_h} (v, \mathcal{Q}_h^{k-1}(\mathcal{L}\Phi) - \mathbf{b} \cdot \mathcal{Q}_h^{k-1}(\nabla \Phi) + c Q_0 \Phi)_T$$

$$= \sum_{T \in \mathcal{T}_h} (v, \mathcal{L}\Phi - \mathbf{b} \cdot \nabla \Phi + c \Phi)_T = \sum_{T \in \mathcal{T}_h} (v, \psi)_T$$
(5.8)

for all $v \in M_h$. From the trace inequality (7.1), the estimate (7.3) with $m = \gamma$, and the estimate (5.6), there holds

$$\sum_{T \in \mathcal{T}_{h}} h_{T}^{-3} \int_{\partial T} |\sigma_{0} - \sigma_{b}|^{2} ds = \sum_{T \in \mathcal{T}_{h}} h_{T}^{-3} \int_{\partial T} |Q_{0} \Phi - Q_{b} \Phi|^{2} ds$$

$$\leq \sum_{T \in \mathcal{T}_{h}} h_{T}^{-3} \int_{\partial T} |Q_{0} \Phi - \Phi|^{2} ds$$

$$\leq \sum_{T \in \mathcal{T}_{h}} C\{h_{T}^{-4} \|Q_{0} \Phi - \Phi\|_{T}^{2} + h_{T}^{2\gamma - 4} \|Q_{0} \Phi - \Phi\|_{\gamma, T}^{2}\}$$

$$\leq Ch^{2\gamma - 2} \sum_{i=1}^{N} \|\Phi\|_{1 + \gamma, \Omega_{i}}^{2} \leq Ch^{2\gamma - 2} \|\psi\|_{\gamma - 1}^{2}.$$

$$(5.9)$$

A similar analysis can be applied to yield the following estimate:

$$\sum_{T \in \mathcal{T}_h} h_T^{-1} \int_{\partial T} |a \nabla \sigma_0 \cdot \mathbf{n} - \boldsymbol{\sigma}_n|^2 ds \le C h^{2\gamma - 2} \|\psi\|_{\gamma - 1}^2. \tag{5.10}$$

Furthermore, by letting $\sigma = Q_h \Phi$ and using (5.6), we arrive at

$$\sum_{T \in \mathcal{T}_{h}} \tau \int_{T} |\sigma_{0}|^{2} dT = \sum_{T \in \mathcal{T}_{h}} \tau \int_{T} |Q_{0}\Phi|^{2} dT$$

$$\leq C \sum_{i=1}^{N} \|\Phi\|_{1+\gamma,\Omega_{i}}^{2} \leq C \|\psi\|_{\gamma-1}^{2}.$$
(5.11)

Combining the estimates (5.9)-(5.11) and then using the definition of $\|\sigma\|_{W}$, we obtain

$$\|\sigma\|_{W}^{2} \le Ch^{2\gamma-2}\|\psi\|_{\gamma-1}^{2}. \tag{5.12}$$

Thus, it follows from (5.8) and (5.12) that

$$\sup_{0 \neq \sigma \in W_h^0} \frac{b(v, \sigma)}{\|\sigma\|_w} \ge \sup_{0 \neq \sigma = Q_h \Phi \in W_h^0} \frac{b(v, \sigma)}{\|\sigma\|_w}$$

$$\ge \sup_{0 \neq \psi \in L^2(\Omega)} \frac{\sum_{T \in \mathcal{T}_h} (v, \psi)_T}{\|Q_h \Phi\|_w}$$

$$\ge \sup_{0 \neq \psi \in L^2(\Omega)} \frac{(v, \psi)}{Ch^{\gamma - 1} \|\psi\|_{\gamma - 1}}$$

$$\ge \beta h^{1 - \gamma} \|v\|_{1 - \gamma},$$

for some constant β independent of the meshsize h. This completes the proof of the lemma. \Box

We are now in a position to state the main result on the solution existence and uniqueness for the primal-dual weak Galerkin finite element method (4.3)-(4.4).

Theorem 5.4. Under the assumption of (5.6), the primal-dual weak Galerkin finite element scheme (4.3)-(4.4) has one and only one solution.

Proof. It is sufficient to show that the homogeneous case of (4.3)-(4.4) has only the trivial solution. To this end, assume f=0, $g_i=0$ for $i=1,\cdots,N$, $\phi_m=0$ and $\psi_m=0$ for $m=1,\cdots,M$ in (4.3)-(4.4). This implies $\phi_h(\sigma)=0$ for all $\sigma\in W_h^0$. By choosing $\sigma=\lambda_h$ and $w=u_h$ in (4.3)-(4.4), we have

$$s(\lambda_h, \lambda_h) = 0$$
,

which gives $\lambda_h \equiv 0$ from Lemma 5.2. The equation (4.3) can then be rewritten as

$$b(u_h, \sigma) = 0, \qquad \forall \sigma \in W_h^0, \tag{5.13}$$

which, together with Lemma 5.3, implies

$$0 = \sup_{0 \neq \sigma \in W_0^0} \frac{b(u_h, \sigma)}{\|\sigma\|_W} \ge \beta h^{1-\gamma} \|u_h\|_{1-\gamma},$$

so that $u_h \equiv 0$ in Ω . This completes the proof of the theorem. \square

6. Error equations

The goal of this section is to derive some error equations for the primal-dual weak Galerkin method (4.3)-(4.4). The error equations shall play a critical role in the forthcoming convergence analysis.

Let u and $(u_h; \lambda_h) \in M_h \times W_h^0$ be the exact solution of the elliptic interface problem (1.1)-(1.4) and its numerical solution arising from the PDWG scheme (4.3)-(4.4). Note that the exact Lagrangian multiplier $\lambda = 0$ is trivial. Denote the error functions by

$$e_h = \mathcal{Q}_h^{k-1} u - u_h, \ e_u = \mathcal{Q}_h^{k-1} u - u,$$
 (6.1)

$$\epsilon_h = Q_h \lambda - \lambda_h = -\lambda_h. \tag{6.2}$$

Lemma 6.1. Let u and $(u_h; \lambda_h) \in M_h \times W_h^0$ be the exact solution of elliptic interface problem (1.1)-(1.4) and its numerical solution arising from the PDWG scheme (4.3)-(4.4). The error functions e_h and ϵ_h defined in (6.1)-(6.2) satisfy the following equations:

$$s(\epsilon_h, \sigma) + b(e_h, \sigma) = \ell_u(\sigma), \quad \forall \sigma \in W_h^0,$$
 (6.3)

$$b(w, \epsilon_h) = 0, \qquad \forall w \in M_h. \tag{6.4}$$

Here

$$\ell_{u}(\sigma) = \sum_{T \in \mathcal{T}_{h}} \langle e_{u}, a \nabla \sigma_{0} \cdot \mathbf{n} - \sigma_{n} \rangle_{\partial T} + (\sigma_{0}, ce_{u})_{T} + \langle \sigma_{b} - \sigma_{0}, (a \nabla e_{u} - \mathbf{b}e_{u}) \cdot \mathbf{n} \rangle_{\partial T}.$$

$$(6.5)$$

Proof. Recalling the definition of $b(\cdot, \cdot)$ in (4.2) and choosing $w = \mathcal{Q}_h^{k-1}u$ in (3.2) and $\psi = \mathbf{b}\mathcal{Q}_h^{k-1}u$ in (3.4), we get

$$\begin{split} b(\mathcal{Q}_h^{k-1}u,\sigma) &= \sum_{T \in \mathcal{T}_h} (\mathcal{Q}_h^{k-1}u,\mathcal{L}_w \sigma - \mathbf{b} \cdot \nabla_w \sigma + c\sigma_0)_T \\ &= \sum_{T \in \mathcal{T}_h} (\sigma_0,\mathcal{L}(\mathcal{Q}_h^{k-1}u))_T + \langle \sigma_b, a \nabla \mathcal{Q}_h^{k-1}u \cdot \mathbf{n} \rangle_{\partial T} - \langle \sigma_n, \mathcal{Q}_h^{k-1}u \rangle_{\partial T} \\ &+ (\sigma_0, \nabla \cdot (\mathbf{b}\mathcal{Q}_h^{k-1}u))_T - \langle \sigma_b, \mathbf{b}\mathcal{Q}_h^{k-1}u \cdot \mathbf{n} \rangle_{\partial T} + (\mathcal{Q}_h^{k-1}u, c\sigma_0)_T. \end{split}$$

Observe that the exact Lagrangian multiplier $\lambda=0$ is trivial, so that $s(Q_h\lambda,\sigma)=0$ for all $\sigma\in W_h^0$. It follows from (1.3) -(1.4) and $\sigma_b|_{\partial\Omega}=0$ that

$$s(Q_{h}\lambda,\sigma) + b(Q_{h}^{k-1}u,\sigma)$$

$$= \sum_{T \in \mathcal{T}_{h}} (\sigma_{0}, \mathcal{L}(Q_{h}^{k-1}u) + \nabla \cdot (\mathbf{b}Q_{h}^{k-1}u) + cQ_{h}^{k-1}u)_{T}$$

$$+ \sum_{T \in \mathcal{T}_{h}} (\langle \sigma_{b}, (a\nabla(Q_{h}^{k-1}u - u) - \mathbf{b}(Q_{h}^{k-1}u - u)) \cdot \mathbf{n} \rangle_{\partial T} - \langle \sigma_{n}, Q_{h}^{k-1}u - u \rangle_{\partial T})$$

$$- \sum_{i=1}^{N} \langle g_{i}, \sigma_{n} \rangle_{\partial \Omega_{i} \cap \partial \Omega} - \sum_{m=1}^{M} \langle \phi_{m}, \sigma_{n} \rangle_{\Gamma_{m}} + \sum_{m=1}^{M} \langle \psi_{m}, \sigma_{b} \rangle_{\Gamma_{m}}.$$

$$(6.6)$$

Denote

$$I = \sum_{T \in \mathcal{T}_h} (\sigma_0, \mathcal{L}(\mathcal{Q}_h^{k-1}u) + \nabla \cdot (\mathbf{b}\mathcal{Q}_h^{k-1}u) + c\mathcal{Q}_h^{k-1}u)_T.$$

By the usual integration by parts, and (1.1)-(1.4), we have

$$\begin{split} I &= \sum_{T \in \mathcal{T}_h} (\sigma_0, \mathcal{L}e_u + \nabla \cdot (\mathbf{b}e_u) + ce_u)_T + (f, \sigma_0) \\ &= \sum_{T \in \mathcal{T}_h} ((a\nabla e_u - \mathbf{b}e_u, \nabla \sigma_0)_T - \langle (a\nabla e_u - \mathbf{b}e_u) \cdot \mathbf{n}, \sigma_0 \rangle_{\partial T}) + (\sigma_0, ce_u + f) \\ &= \sum_{T \in \mathcal{T}_h} (e_u, \mathcal{L}\sigma_0)_T + \langle e_u, a\nabla \sigma_0 \cdot \mathbf{n} \rangle_{\partial T} - (\mathbf{b}e_u, \nabla \sigma_0)_T - \langle (a\nabla e_u - \mathbf{b}e_u) \cdot \mathbf{n}, \sigma_0 \rangle_{\partial T} \\ &+ (\sigma_0, ce_u + f) \\ &= \sum_{T \in \mathcal{T}_h} \langle e_u, a\nabla \sigma_0 \cdot \mathbf{n} \rangle_{\partial T} - \langle (a\nabla e_u - \mathbf{b}e_u) \cdot \mathbf{n}, \sigma_0 \rangle_{\partial T} + (\sigma_0, ce_u + f), \end{split}$$

where we have used $(e_u, \nabla \cdot (a \nabla \sigma_0))_T = 0$ and $(\nabla \sigma_0, \mathbf{b} e_u)_T = 0$ due to the orthogonality property of the L^2 projection operator \mathcal{O}_k^{k-1} .

Substituting the above equation of I into (6.6) yields

$$s(Q_{h}\lambda,\sigma) + b(Q_{h}^{k-1}u,\sigma)$$

$$= \sum_{T \in \mathcal{T}_{h}} \langle e_{u}, a \nabla \sigma_{0} \cdot \mathbf{n} - \sigma_{n} \rangle_{\partial T} + \langle \sigma_{b} - \sigma_{0}, (a \nabla e_{u} - \mathbf{b}e_{u}) \cdot \mathbf{n} \rangle_{\partial T} + (\sigma_{0}, ce_{u} + f)_{T}$$

$$- \sum_{i=1}^{N} \langle g_{i}, \sigma_{n} \rangle_{\partial \Omega_{i} \cap \partial \Omega} - \sum_{m=1}^{M} \langle \phi_{m}, \sigma_{n} \rangle_{\Gamma_{m}} + \sum_{m=1}^{M} \langle \psi_{m}, \sigma_{b} \rangle_{\Gamma_{m}}.$$
(6.7)

The difference of (6.7) and (4.3) gives (6.3).

From $\lambda = 0$, the equation (4.4) gives rise to

$$b(w, \epsilon_h) = b(w, Q_h \lambda - \lambda_h) = b(w, -\lambda_h) = 0, \quad \forall w \in M_h,$$

which completes the derivation of (6.4). The proof is thus completed. \Box

The equations (6.3)-(6.4) are called error equations for the primal-dual WG finite element scheme (4.3)-(4.4).

Remark 6.1. For C^0 -WG elements (i.e., $\sigma_0 = \sigma_b$ on the boundary of each element), the second term in (6.5) vanishes so that $l_u(\sigma)$ can be simplified as

$$\ell_{u}(\sigma) = \sum_{T \in \mathcal{T}_{h}} \langle e_{u}, a \nabla \sigma_{0} \cdot \mathbf{n} - \sigma_{n} \rangle_{\partial T} + (\sigma_{0}, ce_{u})_{T}, \tag{6.8}$$

which involves no derivative for the exact solution u. The expression (6.8) permits an error estimate under ultra-low regularity assumptions for the solution of the interface problem (1.1)-(1.4).

7. Error estimates

As \mathcal{T}_h is a shape-regular finite element partition of the domain Ω , for any $T \in \mathcal{T}_h$ and $\varphi \in H^{\gamma}(T)$ $(\frac{1}{2} < \gamma \le 1)$, the following trace inequality holds true [43]:

$$\|\varphi\|_{\partial T}^{2} \le C(h_{T}^{-1}\|\varphi\|_{T}^{2} + h_{T}^{2\gamma - 1}\|\varphi\|_{Y,T}^{2}). \tag{7.1}$$

Lemma 7.1. [43] Let \mathcal{T}_h be a finite element partition of Ω satisfying the shape regularity assumptions as specified in [43]. The following estimates hold true

$$\sum_{T \in \mathcal{T}_h} h_T^{2l} \| u - \mathcal{Q}_h^{k-1} u \|_{l,T}^2 \le C h^{2m} \| u \|_m^2, \tag{7.2}$$

$$\sum_{T \in \mathcal{T}_{l}} h_{T}^{2l} \|u - Q_{0}u\|_{l,T}^{2} \le Ch^{2(m+1)} \|u\|_{m+1}^{2}, \tag{7.3}$$

where $0 \le l \le 2$ and $0 \le m \le k$.

The main convergence result can be stated as follows.

Theorem 7.2. Assume $k \ge 1$. Let u and $(u_h; \lambda_h) \in M_h \times W_h^0$ be the exact solution of the elliptic interface problem (1.1)-(1.4) and its numerical solution arising from the PDWG scheme (4.3)-(4.4). Assume that u is sufficiently regular such that $u \in \prod_{i=1}^N H^k(\Omega_i) \cap H^{1+\gamma}(\Omega_i)$. The following error estimate holds true:

$$\|\|\epsilon_h\|\|_{w} + h^{1-\gamma} \|e_h\|_{1-\gamma} \le Ch^k \left((1+\tau^{-1}) \sum_{i=1}^N \|u\|_{k,\Omega_i}^2 + \delta_{k,1} h^{2\gamma} \|u\|_{1+\gamma,\Omega_i}^2 \right)^{\frac{1}{2}}, \tag{7.4}$$

where $\frac{1}{2} < \gamma \le 1$ and $\delta_{i,j}$ is the Kronecker delta with value 1 when i=j and 0 otherwise. As a result, one has the following optimal order error estimate in the $H^{1-\gamma}$ -norm for u_h

$$\|u - u_h\|_{1-\gamma} \le Ch^{k+\gamma-1} \left((1+\tau^{-1}) \sum_{i=1}^{N} \|u\|_{k,\Omega_i}^2 + \delta_{k,1} h^{2\gamma} \|u\|_{1+\gamma,\Omega_i}^2 \right)^{\frac{1}{2}}.$$
 (7.5)

Proof. Note that $\epsilon_h = -\lambda_h \in W_h^0$. Choosing $\sigma = \epsilon_h$ and $w = e_h$ in (6.3) and (6.4) gives rise to

$$s(\epsilon_h, \epsilon_h) = \ell_u(\epsilon_h).$$
 (7.6)

For $k \ge 2$, we use (7.6), the Cauchy-Schwarz inequality, the equation (6.5), the trace inequality (7.1), and the estimates (7.2) with m = k to obtain

$$\begin{split} &\|\boldsymbol{\epsilon}_{h}\|_{W}^{2} = s(\boldsymbol{\epsilon}_{h}, \boldsymbol{\epsilon}_{h}) = |\ell_{u}(\boldsymbol{\epsilon}_{h})| \\ &\leq \Big(\sum_{T \in \mathcal{T}_{h}} h_{T}^{-3} \|\boldsymbol{\epsilon}_{0} - \boldsymbol{\epsilon}_{b}\|_{\partial T}^{2}\Big)^{\frac{1}{2}} \Big(\sum_{T \in \mathcal{T}_{h}} h_{T}^{3} \|(a\nabla e_{u} - \mathbf{b}e_{u}) \cdot \mathbf{n}\|_{\partial T}^{2}\Big)^{\frac{1}{2}} \\ &+ \Big(\sum_{T \in \mathcal{T}_{h}} h_{T}^{-1} \|a\nabla \boldsymbol{\epsilon}_{0} \cdot \mathbf{n} - \boldsymbol{\epsilon}_{n}\|_{\partial T}^{2}\Big)^{\frac{1}{2}} \Big(\sum_{T \in \mathcal{T}_{h}} h_{T} \|e_{u}\|_{\partial T}^{2}\Big)^{\frac{1}{2}} \\ &+ \Big(\sum_{T \in \mathcal{T}_{h}} \tau \|\boldsymbol{\epsilon}_{0}\|_{T}^{2}\Big)^{\frac{1}{2}} \Big(\sum_{T \in \mathcal{T}_{h}} \tau^{-1} \|ce_{u}\|_{T}^{2}\Big)^{\frac{1}{2}} \\ &\leq C \|\|\boldsymbol{\epsilon}_{h}\|_{W} \left(\sum_{T \in \mathcal{T}_{h}} h_{T}^{2} \|a\nabla e_{u} - \mathbf{b}e_{u}\|_{T}^{2} + h_{T}^{2\gamma+2} \|a\nabla e_{u} - \mathbf{b}e_{u}\|_{\gamma,T}^{2} \\ &+ \|e_{u}\|_{T}^{2} + h_{T}^{2\gamma} \|e_{u}\|_{\gamma,T}^{2} + \tau^{-1} \|ce_{u}\|_{T}^{2}\Big)^{\frac{1}{2}} \,. \end{split}$$

Therefore, for $k \ge 2$, we have

$$\|\|\epsilon_h\|\|_W^2 \le Ch^k \left((1+\tau^{-1}) \sum_{i=1}^N \|u\|_{k,\Omega_i}^2 \right)^{\frac{1}{2}} \|\|\epsilon_h\|\|_W.$$

As to the case k = 1, we have $\nabla Q_h^{k-1} u = 0$ and thus

$$\begin{split} \left\| \left\| \epsilon_h \right\|_{w}^{2} & \leq C \bigg(\sum_{T \in \mathcal{T}_h} h_{T}^{2} \| a \nabla u - \mathbf{b} e_u \|_{T}^{2} + h_{T}^{2\gamma + 2} \| a \nabla u - \mathbf{b} e_u \|_{\gamma, T}^{2} \\ & + \left\| e_u \right\|_{T}^{2} + h_{T}^{2\gamma} \left\| e_u \right\|_{\gamma, T}^{2} + \tau^{-1} \left\| c e_u \right\|_{T}^{2} \bigg)^{\frac{1}{2}}, \\ & \leq C h \left((1 + \tau^{-1}) \sum_{i=1}^{N} \left\| u \right\|_{1, \Omega_{i}}^{2} + h^{2\gamma} \left\| u \right\|_{1 + \gamma, \Omega_{i}}^{2} \right)^{\frac{1}{2}}. \end{split}$$

Consequently, there holds for all $k \ge 1$

$$\|\|\epsilon_h\|\|_{w} \le Ch^k \left((1+\tau^{-1}) \sum_{i=1}^N \|u\|_{k,\Omega_i}^2 + \delta_{k,1} h^{2\gamma} \|u\|_{1+\gamma,\Omega_i}^2 \right)^{\frac{1}{2}}.$$

$$(7.7)$$

As to the estimate for the error function e_h , we use the error equation (6.3), (7.7), the Cauchy-Schwarz inequality, and the triangle inequality to obtain

$$\begin{split} |b(e_h,\sigma)| &= |\ell_u(\sigma) - s(\epsilon_h,\sigma)| \le |\ell_u(\sigma)| + \|\epsilon_h\|_w \|\sigma\|_w \\ &\le Ch^k \left((1+\tau^{-1}) \sum_{i=1}^N \|u\|_{k,\Omega_i}^2 + \delta_{k,1} h^{2\gamma} \|u\|_{1+\gamma,\Omega_i}^2 \right)^{\frac{1}{2}} \|\sigma\|_w, \end{split}$$

which, combined with the inf-sup condition (5.7), yields the following error estimate

$$\beta h^{1-\gamma} \|e_h\|_{1-\gamma} \le C h^k \left((1+\tau^{-1}) \sum_{i=1}^N \|u\|_{k,\Omega_i}^2 + \delta_{k,1} h^{2\gamma} \|u\|_{1+\gamma,\Omega_i}^2 \right)^{\frac{1}{2}}.$$
 (7.8)

Then the desired error estimate (7.4) follows from (7.7) and (7.8). Finally, the estimate (7.5) is a direct result of (7.4) and the triangle inequality. This completes the proof of the theorem. \Box

Corollary 7.3. Assume $k \ge 1$. Let u and $(u_h; \lambda_h) \in M_h \times W_h^0$ be the exact solution of the elliptic interface problem (1.1)-(1.4) and its numerical solution arising from the PDWG scheme (4.3)-(4.4). Assume that the exact solution u has the "low" regularity of $u \in \prod_{i=1}^N H^\delta(\Omega_i)$ for some $\frac{1}{2} < \delta \le k$. Then, for C^0 -WG elements, the following error estimate holds true:

$$\|\|\epsilon_h\|\|_w + h^{1-\gamma} \|e_h\|_{1-\gamma} \le Ch^{\delta} (1+\tau^{-1})^{\frac{1}{2}} \left(\sum_{i=1}^N \|u\|_{\delta,\Omega_i}^2 \right)^{\frac{1}{2}}, \tag{7.9}$$

where $\frac{1}{2} < \gamma \le 1$ is related to the regularity estimate (5.6). Consequently, one has the following error estimate

$$||u - u_h||_{1 - \gamma} \le Ch^{\delta + \gamma - 1} (1 + \tau^{-1})^{\frac{1}{2}} \left(\sum_{i=1}^{N} ||u||_{\delta, \Omega_i}^2 \right)^{\frac{1}{2}}.$$

$$(7.10)$$

Proof. It is easy to see $\epsilon_h \in W_h^0$. By letting $\sigma = \epsilon_h$ and $w = e_h$ in (6.3) and (6.4) we arrive at

$$s(\epsilon_h, \epsilon_h) = \ell_u(\epsilon_h). \tag{7.11}$$

Now, we use (7.11), the Cauchy-Schwarz inequality, the equation (6.8), the trace inequality (7.1), and the estimates (7.2) with $m = \delta$ to obtain

$$\|\|\boldsymbol{\epsilon}_h\|\|_{w}^{2} = s(\boldsymbol{\epsilon}_h, \boldsymbol{\epsilon}_h) = |\ell_u(\boldsymbol{\epsilon}_h)|$$

$$\leq \left(\sum_{T \in \mathcal{T}_h} h_T^{-1} \|a\nabla \boldsymbol{\epsilon}_0 \cdot \mathbf{n} - \boldsymbol{\epsilon}_n\|_{\partial T}^{2}\right)^{\frac{1}{2}} \left(\sum_{T \in \mathcal{T}_h} h_T \|\boldsymbol{e}_u\|_{\partial T}^{2}\right)^{\frac{1}{2}}$$

$$\begin{split} & + \Big(\sum_{T \in \mathcal{T}_h} \tau \, \|\epsilon_0\|^2\Big)^{\frac{1}{2}} \Big(\sum_{T \in \mathcal{T}_h} \tau^{-1} \|ce_u\|_T^2\Big)^{\frac{1}{2}} \\ & \leq C \|\epsilon_h\|_w \Big(\sum_{T \in \mathcal{T}_h} \|e_u\|_T^2 + h_T^{2\gamma} \|e_u\|_{\gamma,T}^2 + \tau^{-1} \|ce_u\|_T^2\Big)^{\frac{1}{2}} \\ & \leq C \|\epsilon_h\|_w h^{\delta} (1 + \tau^{-1})^{\frac{1}{2}} \left(\sum_{i=1}^N \|u\|_{\delta,\Omega_i}^2\right)^{\frac{1}{2}}. \end{split}$$

Hence,

$$\|\|\epsilon_h\|\|_{w} \le Ch^{\delta} (1+\tau^{-1})^{\frac{1}{2}} \left(\sum_{i=1}^{N} \|u\|_{\delta,\Omega_i}^2 \right)^{\frac{1}{2}}. \tag{7.12}$$

As to the estimate for e_h , we use the error equation (6.3), (7.12), the Cauchy-Schwarz inequality, and the triangle inequality to obtain

$$\begin{split} |b(e_h,\sigma)| &= |\ell_u(\sigma) - s(\epsilon_h,\sigma)| \leq |\ell_u(\sigma)| + \|\epsilon_h\|_w \|\sigma\|_w \\ &\leq Ch^\delta (1+\tau^{-1})^{\frac{1}{2}} \|\sigma\|_w \left(\sum_{i=1}^N \|u\|_{\delta,\Omega_i}^2\right)^{\frac{1}{2}}, \end{split}$$

which, combined with the inf-sup condition (5.7), gives rise to the following error estimate

$$\beta h^{1-\gamma} \|e_h\|_{1-\gamma} \le Ch^{\delta} (1+\tau^{-1})^{\frac{1}{2}} \left(\sum_{i=1}^{N} \|u\|_{\delta,\Omega_i}^2 \right)^{\frac{1}{2}}. \tag{7.13}$$

The desired error estimate (7.9) then follows from (7.12) and (7.13). Finally, (7.10) is a direct consequence of (7.9) and the triangle inequality. This completes the proof of the theorem. \Box

8. Numerical experiments

In this section, we will present some numerical results to verify the efficiency and accuracy of the proposed primal-dual weak Galerkin method (4.3)-(4.4) for solving the elliptic interface problem (1.1)-(1.4). In our experiments, we shall implement the algorithm with k=1,2 in the finite element spaces M_h and W_h^0 . We shall compute various approximation errors for u_h and λ_h , including the L^2 error $\|u-u_h\|_0$ and $\|\lambda_0\|_0$, the H^1 error $\|\lambda_0\|_1$ for λ_h , and the discrete error $\|\lambda_h\|_W$ as defined by (5.3). If not otherwise stated, the parameter τ in the PDWG numerical scheme will be $\tau=1$. The finite element partition \mathcal{T}_h is obtained through a successive refinement of a coarse triangulation of the domain in aligning with the interface, by dividing each coarse element into four congruent sub-elements by connecting the mid-points of the three edges of the triangle. When the curved interface segments are involved, we use the straight-line to approximate curved interface segments. To diminish this approximation error and ensure the accuracy of the numerical solution, the computational interface of the initial mesh should be carefully taken. For example, for higher-order polynomial approximation, we may choose a higher-order straight-line approximation (e.g., a finer mesh near the curved interface). The right-hand side functions, the boundary and interface conditions are all derived from the exact solution.

Example 1: We consider the interface problem (1.1)-(1.4) on the domain $\Omega = (0, 1)^2$ with an interface given by $\Omega_1 = [0.25, 0.75]^2$ and $\Omega_2 = \Omega \setminus \Omega_1$. The coefficients in the model equations are taken as

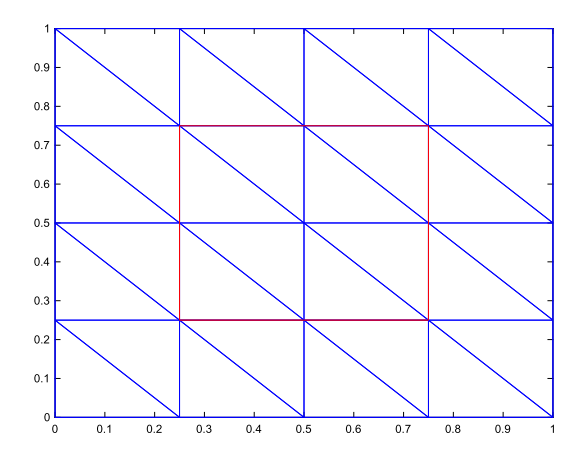
$$a_1 = a_2 = 1$$
, $\mathbf{b}_1 = \mathbf{b}_2 = (1, 1)$, $c_1 = c_2 = 1$.

The analytical solution to the elliptic equation is given as

$$u = \begin{cases} 10 - x^2 - y^2 & \text{if } (x, y) \in \Omega_1, \\ \sin(\pi x) \sin(\pi y) & \text{if } (x, y) \in \Omega_2. \end{cases}$$

The initial mesh is shown in Fig. 8.1 (left one). The mesh refinement of the previous level is done by connecting the midpoints of the edges. The mesh at the next level is illustrated in Fig. 8.1 (right one). The surface plot of the PDWG solution u_h on the finest mesh (i.e., after the fifth refinement of the initial mesh) is depicted in Fig. 8.2.

Table 8.1 shows the numerical results and the rate of convergence for k = 1, 2. We observe that, for both linear (k = 1) and quadratic (k = 2) PDWG methods, the convergence rate for the errors $||u - u_h||_0$ and $||\lambda_h||_w$ is of $\mathcal{O}(h^k)$, which is consistent with the theoretical estimate (7.4) in Theorem 7.2. As to the approximation error for λ_0 , we observe a convergence



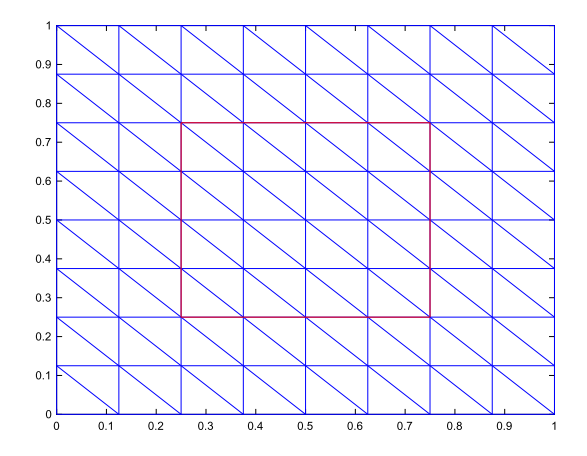


Fig. 8.1. The initial mesh (left) and the next level refinement (right).

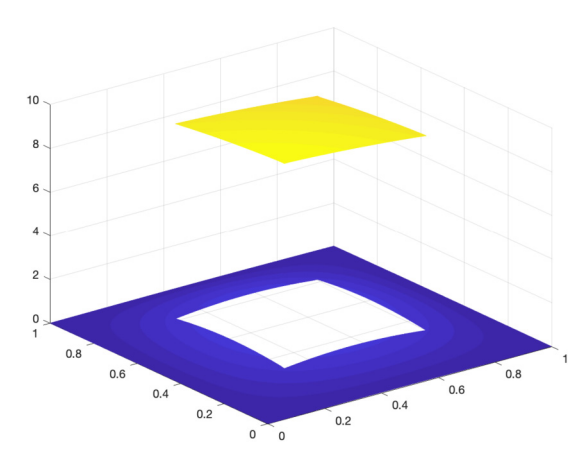


Fig. 8.2. Surface plot of the numerical solution u_h calculated by the PDWG method of Example 1.

Table 8.1Errors and convergence rates of the linear and quadratic PDWG methods for Example 1.

	h	$\ \lambda_h\ _w$	rate	$\ \lambda_0\ _1$	rate	$\ \lambda_0\ _0$	rate	$ u-u_h _0$	rate
	2.50e-1	1.15e-0	-	2.56e-1	-	1.21e-1	-	1.74e-1	_
	1.25e-1	6.32e-1	0.87	9.52e-2	1.43	3.56e-2	1.77	7.78e-2	1.16
k = 1	6.25e-2	3.34e-1	0.92	3.01e-2	1.66	9.73e-3	1.87	3.51e-2	1.15
	3.13e-2	1.72e-1	0.96	8.49e-3	1.82	2.54e-3	1.94	1.66e-2	1.09
	1.56e-2	8.73e-2	0.98	2.26e-3	1.92	6.47e-4	1.97	8.06e-3	1.04
	h	$\ \lambda_h\ _w$	rate	$\ \lambda_0\ _1$	rate	$\ \lambda_0\ _0$	rate	$ u-u_h _0$	rate
	h 2.50e-1	$\ \lambda_h\ _{w}$ 2.00e-1	rate -	λ ₀ ₁ 1.88e-2	rate -	λ ₀ ₀ 5.71e-3	rate -	$ u - u_h _0$ 2.80e-2	rate -
					rate - 3.56				rate - 2.07
k = 2	2.50e-1	2.00e-1	_	1.88e-2	_	5.71e-3	-	2.80e-2	
k = 2	2.50e-1 2.50e-1	2.00e-1 5.12e-2	- 1.97	1.88e-2 1.59e-3	- 3.56	5.71e-3 3.61e-4	3.98	2.80e-2 6.66e-3	2.07

rate of $\mathcal{O}(h^{k+1})$ for $\|\lambda_0\|_1$ from this numerical experiment, which suggests a superconvergence for the dual variable λ_0 in the H^1 -norm. We further observe a convergence of order $\mathcal{O}(h^{k+1})$ for k=1 and of h^{k+2} for k=2 for λ_0 in the L^2 norm. Again, the (k+2)-th order of convergence for $\|\lambda_0\|_0$ indicates a pleasant superconvergence phenomenon of the PDWG method.

To test the condition number of the PDWG scheme and its dependency on the coefficient contrast, we consider different choices of coefficient contrasts in five cases:

- Case 1: $a_1 = a_2 = 1$, $\mathbf{b}_1 = \mathbf{b}_2 = (1, 1)$, $c_1 = c_2 = 1$.
- Case 2: $a_1 = 100$, $a_2 = 1$, $\mathbf{b}_1 = \mathbf{b}_2 = (1, 1)$, $c_1 = c_2 = 1$.
- Case 3: $a_1 = 1000, a_2 = 1, \quad \mathbf{b}_1 = \mathbf{b}_2 = (1, 1), \quad c_1 = c_2 = 1.$

Condition numbers and growth rates of the matrix calculated from the linear PDWG in different choices of parameters with a rectangular interface.

case 1	h^{-p}	case 2	h^{-p}	case 3	h^{-p}	case 4	h^{-p}	case 5	h^{-p}
1.92e+4	-	4.14e+6	-	4.07e+8	-	2.05e+4	-	1.86e+5	_
2.97e+5	3.95	6.26e+6	0.60	6.06e+8	0.57	1.02e+5	2.31	3.16e+5	0.77
5.33e+6	4.17	3.85e+7	2.62	3.50e+9	2.53	2.90e+6	4.83	4.18e+6	3.73
9.61e+7	4.17	2.56e+8	2.73	1.85e+10	2.40	5.18e+7	4.16	8.45e+7	4.34
1.60e+9	4.06	2.11e+9	3.04	8.38e+10	2.18	9.05e+8	4.13	1.87e+9	4.47

Table 8.3 Condition numbers and growth rates of the matrix calculated from the linear PDWG in different choices of parameters with a circular interface.

case 1	h^{-p}	case 2	h^{-p}	case 3	h^{-p}	case 4	h ^{-p}	case 5	h ^{-p}
3.63e+5	-	1.70e+7	-	1.67e+9	-	3.34e+5	-	5.13e+5	-
2.58e+6	2.83	2.57e+7	0.60	2.47e+9	0.57	1.88e+6	2.50	3.20e+6	2.64
4.70e+7	4.19	1.30e+8	2.33	1.13e+10	2.19	3.50e+7	4.22	6.55e+7	4.36
7.48e+8	3.99	1.16e+9	3.16	5.65e+10	2.33	6.32e+8	4.17	1.41e+9	4.43
1.25e+10	4.07	1.51e+10	3.71	2.48e+11	2.13	1.06e+10	4.07	3.54e+10	4.65

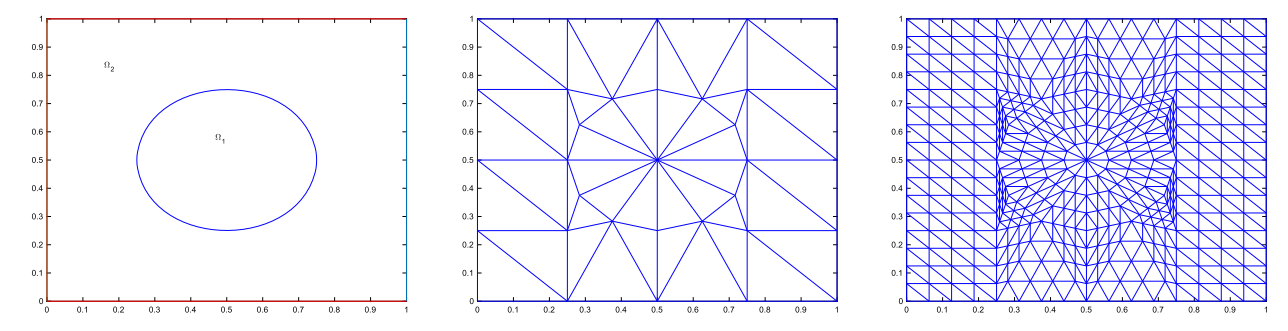


Fig. 8.3. The interface and subdomains (left) and the initial mesh (middle) and the refined mesh from the twice refinement of the initial mesh (right).

- Case 4: $a_1 = 1$, $a_2 = 1$, $\mathbf{b}_1 = \mathbf{b}_2 = (1, 1)$, $c_1 = 1$, $c_2 = 1000$. Case 5: $a_1 = 1$, $a_2 = 1$, $\mathbf{b}_1 = (1000, 1000)$, $\mathbf{b}_2 = (1, 1)$, $c_1 = 1$, $c_2 = 1$.

Listed in Tables 8.2 and 8.3 are the condition numbers and their growth rates of the matrix calculated from the linear PDWG under a rectangular interface and a circular interface, respectively. Here the circular interface and the mesh are the same as these in Example 2. One can see that the condition number grows like $\mathcal{O}(h^{-p})$ for some positive value $p, 2 \le p < 5$ as the mesh size h decreases, which is similar to that of the mixed finite element method for elliptic equations, see, e.g., [34], while is different from the standard finite element method, whose condition number grows like $O(h^{-2})$. Moreover, it seems that the coefficient contrast has effect on the condition number. As the ratio $\frac{a_1}{a_2}$ increases (case 2 and case 3), we see a larger condition number while a smaller growth rate. As the ratio $\frac{c_1}{c_2}$ increases (case 4), the condition number and its growth rate change little and the growth rate remains $\mathcal{O}(h^{-4})$. While we observe a slightly larger growth rate when the coefficient contrast $\frac{b_1}{b_2}$ increases (case 5). In other words, it seems that the convection coefficient contrast and the diffusion coefficient contrast may have different (positive or negative) impacts on the growth rate of the condition number.

Example 2: We consider a circular interface problem on the domain $\Omega = (0, 1)^2$. Here Ω_1 is the disc centered at the point (0.5, 0.5) with radius r = 0.25, and $\Omega_2 = \Omega \setminus \Omega_1$. The coefficients are taken as

$$a_1 = a_2 = 2 + \sin(x + y)$$
, $\mathbf{b}_1 = \mathbf{b}_2 = (x, y)$, $c_1 = c_2 = 4 + x$.

The analytical solution to the interface problem is

$$u = \begin{cases} \sin(x + y) + \cos(x + y) + 5, & \text{if } (x, y) \in \Omega_1, \\ x + y + 1, & \text{if } (x, y) \in \Omega_2. \end{cases}$$

We plot in Fig. 8.3 the interface and subdomains (left), the initial mesh (middle), and the refined mesh generated from twice refinement of the initial mesh (right), respectively. The surface plot of the approximate solution u_h calculated by the PDWG method with k = 1 on the finest mesh is shown in Fig. 8.4.

We present in Table 8.4 the approximation errors and corresponding convergence rates for the primal variable u_h and dual variable λ_h , from which we observe a convergence rate of $\mathcal{O}(h^k)$ for both $\|u-u_h\|_0$ and $\|\lambda_h\|_w$. In other words, the

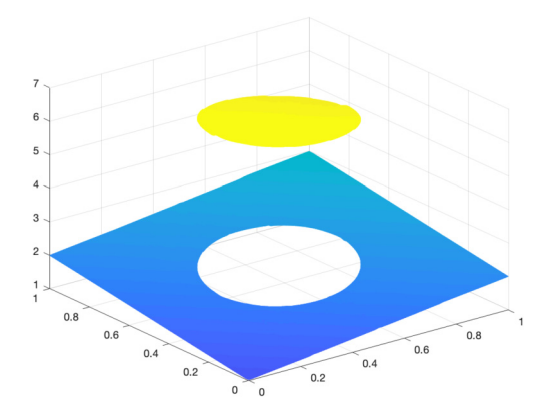


Fig. 8.4. Surface plot of the numerical solution u_h calculated by the PDWG method of Example 2.

Table 8.4Errors and convergence rates of the linear and quadratic PDWG methods for Example 2.

	h	$\ \lambda_h\ _w$	rate	$\ \lambda_0\ _1$	rate	$\ \lambda_0\ _0$	rate	$\ u-u_h\ _0$	rate
	1.29e-1	6.43e-1	-	3.02e-1	-	2.15e-2	-	7.50e-2	-
	6.47e-2	3.55e-1	0.86	9.31e-2	1.70	5.17e-3	2.06	3.75e-2	0.99
k = 1	3.24e-2	1.98e-1	0.84	2.97e-2	1.65	1.42e-3	1.87	1.77e-2	1.09
	1.62e-2	1.07e-1	0.89	8.85e-3	1.75	3.80e-4	1.90	8.35e-3	1.09
	8.09e-3	5.59e-2	0.94	2.43e-3	1.87	9.98e-5	1.93	4.04e-3	1.05
	h	$\ \lambda_h\ _W$	rate	$\ \lambda_0\ _1$	rate	$\ \lambda_0\ _0$	rate	$\ u-u_h\ _0$	rate
	h 1.29e-1	λ _h _w 4.51e-2	rate -	λ ₀ ₁ 6.20e-4	rate -	λ ₀ ₀ 5.44e-4	rate -	$ u - u_h _0$ 3.28e-3	rate -
			rate - 1.99					11 17.11-	rate - 1.98
k = 2	1.29e-1	4.51e-2	-	6.20e-4	-	5.44e-4	-	3.28e-3	-
k = 2	1.29e-1 6.47e-2	4.51e-2 1.14e-2	- 1.99	6.20e-4 5.48e-5	- 3.50	5.44e-4 3.43e-5	- 4.00	3.28e-3 8.30e-4	- 1.98

error bound given in (7.4) is sharp. Analogous to Example 1, we see the error $\|\lambda_0\|_1$ converges to zero with an order of k+1 for both linear and quadratic PDWG methods. Table 8.4 also shows a convergence of λ_0 with order (k+1) for k=1 and (k+2) for k=2 in L^2 norm.

Example 3: The interface problem (1.1)-(1.4) is defined on the domain $\Omega = (0, 1)^2$ with a closed interface Γ parameterized as follows

$$r = 0.5 + \frac{3\sin(3\theta)}{4}.$$

The subdomain Ω_1 is given by the region bounded by the curve Γ and $\Omega_2 = \Omega \setminus \Omega_1$ is the portion of the domain outside Γ . The PDE coefficients are given by

$$a_1 = 1 + x + y$$
, $a_2 = 1$, $\mathbf{b}_1 = \mathbf{b}_2 = (1, 1 + y)$, $c_1 = c_2 = 2$.

The exact solution to the elliptic problem is given as

$$u = \begin{cases} e^{x} \cos(y) + 10, & \text{if } (x, y) \in \Omega_{1}, \\ 5e^{-x^{2} - y^{2}}, & \text{if } (x, y) \in \Omega_{2}. \end{cases}$$

The interface and subdomains, the initial mesh, and the refined mesh after two successive refinements of the initial mesh are shown in Fig. 8.5. The numerical solution u_h calculated by the PDWG method with k=2 on the refined mesh are depicted in Fig. 8.6. The numerical errors of the linear and quadratic PDWG methods are reported in Table 8.5. It can be seen that the theoretical convergence (i.e., $\mathcal{O}(h^k)$ for both $\|u-u_h\|_0$ and $\|\lambda_h\|_W$) is achieved in this numerical test. Moreover, a convergence of $\mathcal{O}(h^{k+1})$ for $\|\lambda_0\|_1$, and $\mathcal{O}(h^{k+1})$ and $\mathcal{O}(h^{k+2})$ for the error $\|\lambda_0\|_0$ is observed for the case of k=1 and k=2, respectively.

Example 4: The interface Γ on the domain $\Omega = (0, 1)^2$ is characterized by the following equation in the polar coordinates:

$$x(\theta) = (1/2 + 1/2\cos(m\theta)\sin(n\theta))\cos(\theta),$$

$$y(\theta) = (1/2 + 1/2\cos(m\theta)\sin(n\theta))\sin(\theta),$$

where m=2 and n=6. The subdomain Ω_1 is the region inside Γ and $\Omega_2=\Omega\backslash\Omega_1$. The coefficients in the elliptic interface problem are given by

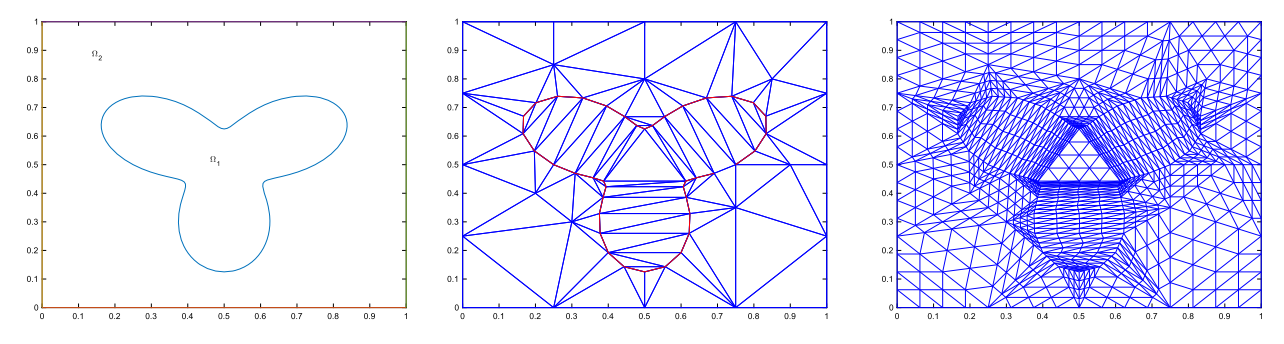


Fig. 8.5. The interface and subdomains (left) and the initial mesh (middle) and the refined mesh (right).

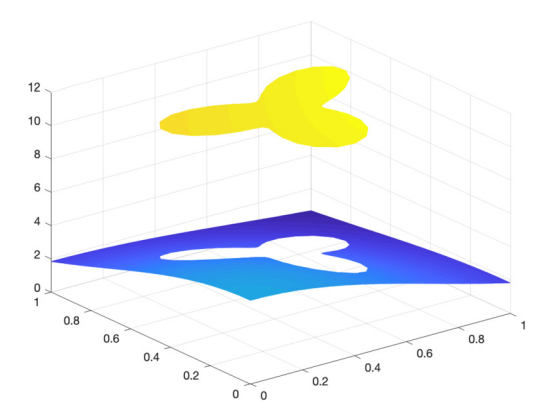


Fig. 8.6. Surface plot of the numerical solution u_h calculated by the PDWG method of Example 3.

Table 8.5Errors and convergence rates of the linear and quadratic PDWG methods for Example 3.

	h	$\ \lambda_h\ _w$	rate	$\ \lambda_0\ _1$	rate	$\ \lambda_0\ _0$	rate	$\ u-u_h\ _0$	rate
	3.54e-1	1.35e-0	-	3.77e-1	-	6.52e-2	-	2.38e-1	_
	1.77e-1	7.32e-1	0.81	1.26e-1	1.58	1.65e-2	1.98	1.25e-1	0.93
k = 1	8.84e-2	4.01e-1	0.87	4.14e-2	1.61	4.37e-3	1.92	6.63e-2	0.92
	4.42e-2	2.16e-1	0.89	1.29e-2	1.68	1.17e-3	1.90	3.54e-2	0.91
	2.21e-2	1.14e-1	0.92	3.75e-3	1.78	3.07e-4	1.93	1.90e-2	0.90
	h	$\ \lambda_h\ _w$	rate	$\ \lambda_0\ _1$	rate	$\ \lambda_0\ _0$	rate	$\ u-u_h\ _0$	rate
	h 3.54e-1	$\ \lambda_h\ _{w}$ 2.01e-1	rate -	λ ₀ ₁ 1.09e-2	rate -	$\ \lambda_0\ _0$ 5.82e-3	rate -	$ u - u_h _0$ 1.66e-2	rate -
									rate - 2.01
k = 2	3.54e-1	2.01e-1	_	1.09e-2	-	5.82e-3	-	1.66e-2	
k = 2	3.54e-1 1.77e-1	2.01e-1 5.12e-2	- 1.97	1.09e-2 9.70e-4	- 3.50	5.82e-3 3.76e-4	- 3.95	1.66e-2 4.13e-3	2.01

$$a_1 = (xy+2)/5$$
, $a_2 = (x^2 - y^2 + 3)/7$, $\mathbf{b}_1 = (0,1)$, $\mathbf{b}_2 = (1,0)$, $c_1 = 2$, $c_2 = 1$.

The exact solution to the interface problem is

$$u = \begin{cases} x + y + 2, & \text{if } (x, y) \in \Omega_1, \\ 0.5 \sin(x + y) + 0.5 \cos(x + y) + 0.3, & \text{if } (x, y) \in \Omega_2. \end{cases}$$

The interface and subdomains are shown in the left of Fig. 8.7. To approximate the curved interface, we consider two types of computational interface in our numerical experiment. The first one is obtained by equally dividing the interval $[0, 2\pi]$ with 20 subintervals, and the corresponding mesh is referred as to Mesh 1. While the second one is derived by using 40 uniformly distributed points and the corresponding mesh is referred as to Mesh 2. The two types of computational interface are shown in the middle and right of Fig. 8.7. We use the Matlab *delaunay* to get the initial mesh. The PDWG solution u_h on the finest mesh are depicted in Fig. 8.8.

The numerical errors of the linear and quadratic PDWG method in two different meshes are reported in Tables 8.6 and 8.7. As we may observe, the errors calculated from Mesh 1 are larger than those from Mesh 2, due to the fact that Mesh 2 provides a better approximation to the curved interface. While the convergence rates for both meshes are almost the same. To be more precise, the numerical convergence rate for $\|\lambda_h\|_W$, $\|u-u_h\|_0$, and $\|\lambda_0\|_1$ are seen to be $\mathcal{O}(h^k)$, $\mathcal{O}(h^k)$, $\mathcal{O}(h^{k+1})$,

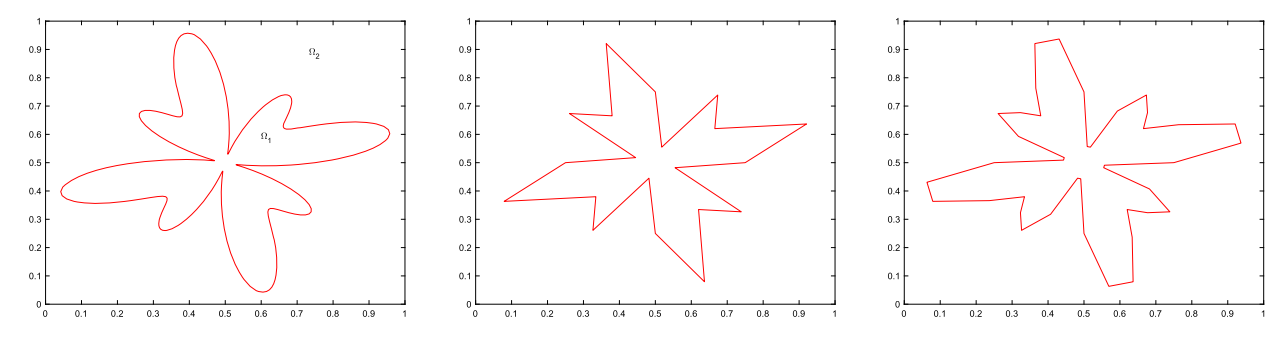


Fig. 8.7. The interface and subdomains (left) and the computational interface at the first stage of Mesh 1 (middle) and Mesh 2 (right).

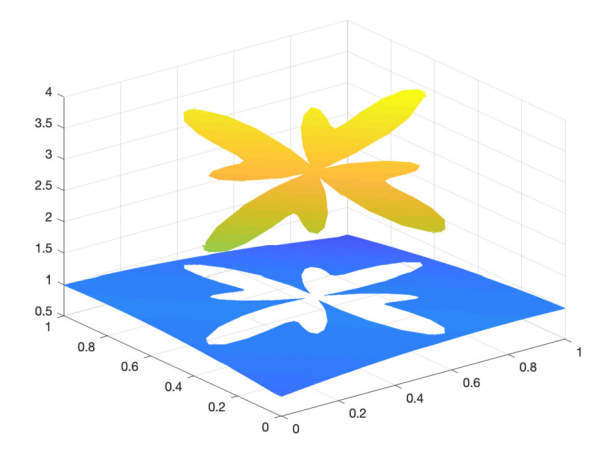


Fig. 8.8. Surface plot of the numerical solution u_h calculated by the PDWG method of Example 4.

Table 8.6Errors and convergence rates of the linear PDWG methods for Example 4 in two different meshes.

	h	$\ \lambda_h\ _w$	rate	$\ \lambda_0\ _1$	rate	$\ \lambda_0\ _0$	rate	$\ u-u_h\ _0$	rate
	3.54e-1	1.58e-1	_	2.94e-2	-	7.35e-3	-	4.02e-2	-
	1.77e-1	8.12e-2	0.96	9.08e-3	1.70	1.79e-3	2.04	1.94e-2	1.05
Mesh 1	8.84e-2	4.15e-2	0.97	2.93e-3	1.63	4.59e-4	1.97	9.55e-3	1.03
	4.42e-2	2.14e-2	0.96	8.58e-4	1.77	1.20e-4	1.93	4.77e-3	1.00
	2.21e-2	1.09e-2	0.97	2.35e-4	1.87	3.06e-5	1.98	2.51e-3	0.93
	3.54e-1	1.24e-1	_	1.96e-2	-	5.72e-3	-	3.15e-2	-
	1.77e-1	6.54e-2	0.92	6.55e-3	1.58	1.44e-3	1.99	1.55e-2	1.03
Mesh 2	8.84e-2	3.48e-2	0.91	2.11e-3	1.64	3.85e-4	1.90	7.77e-3	0.99
	4.42e-2	1.82e-2	0.94	6.23e-4	1.76	1.02e-4	1.91	3.88e-3	1.00
	2.21e-2	9.32e-3	0.96	1.69e-4	1.88	2.62e-5	1.96	1.94e-3	1.00

respectively. Once again, the numerical experiment suggests a convergence at the optimal order of $\mathcal{O}(h^{k+1})$ for $\|\lambda_0\|_0$ for the linear PDWG method and a superconvergence of $\mathcal{O}(h^{k+2})$ for the quadratic PDWG method. As indicated from Tables 8.6 and 8.7, the computation interface of Mesh 1 seems enough to ensure the desired convergence rates for k = 1, 2 in this case. See also Fig. 8.8.

Example 5: We consider an interface problem on the domain $\Omega = (0, 1)^2$ with an interface Γ parameterized in the polar angle θ as follows

$$r = 0.5 + \frac{\sin(5\theta)}{7}.$$

The subdomain Ω_1 is the part inside Γ and $\Omega_2 = \Omega \setminus \Omega_1$ is the part outside Γ . The coefficients in the PDE are given by

$$a_1 = 0.01, \ a_2 = 0.1, \ \mathbf{b}_1 = \mathbf{b}_2 = (0, 0), \ c_1 = c_2 = 0.$$

The exact solution to the elliptic interface problem is

$$u = \begin{cases} e^{(2x-1)^2 + (2y-1)^2}, & \text{if } (x, y) \in \Omega_1, \\ 0.1(x^2 + y^2)^2 - 0.01 \ln(2\sqrt{x^2 + y^2}), & \text{if } (x, y) \in \Omega_2. \end{cases}$$

Table 8.7
Errors and convergence rates of the quadratic PDWG methods for Example 4 in two different meshes.

	h	$\ \lambda_h\ _w$	rate	$\ \lambda_0\ _1$	rate	$\ \lambda_0\ _0$	rate	$\ u-u_h\ _0$	rate
	3.54e-1	1.42e-2	-	1.78e-3	-	3.11e-4	-	2.25e-3	-
	1.77e-1	3.59e-3	1.99	1.93e-4	3.21	1.97e-5	3.98	5.53e-4	2.02
Mesh 1	8.84e-2	8.97e-4	2.00	2.23e-5	3.11	1.24e-6	3.99	1.36e-4	2.02
	4.42e-2	2.24e-4	2.00	2.70e-6	3.05	7.76e-8	4.00	3.39e-5	2.01
	h	$\ \lambda_h\ _w$	rate	$\ \lambda_0\ _1$	rate	$\ \lambda_0\ _0$	rate	$\ u-u_h\ _0$	rate
	h 3.54e-1	λ _h _w 1.26e-2	rate -	λ ₀ ₁ 1.61e-3	rate -	λ ₀ ₀ 2.50e-4	rate -	$ u - u_h _0$ 1.93e-3	rate -
			rate - 2.01						rate - 1.99
Mesh 2	3.54e-1	1.26e-2	-	1.61e-3	-	2.50e-4	-	1.93e-3	

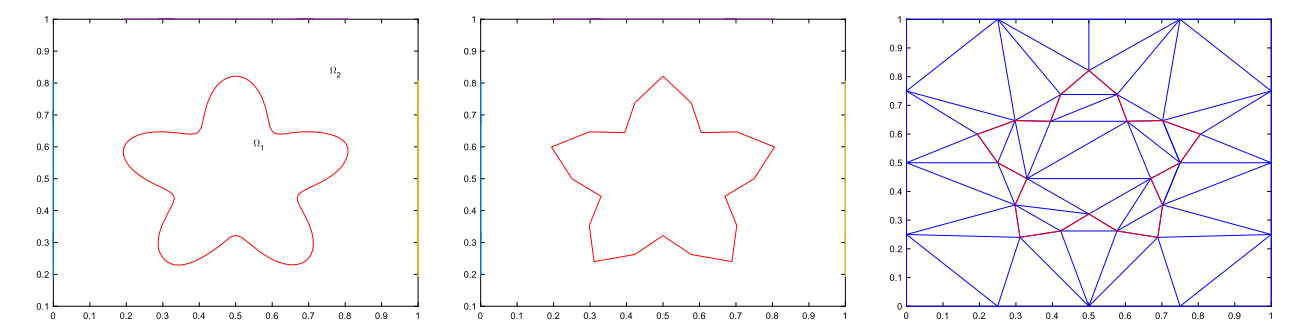


Fig. 8.9. The interface and subdomains (left) and the computation interface at the first stage (middle) and the initial mesh (right).

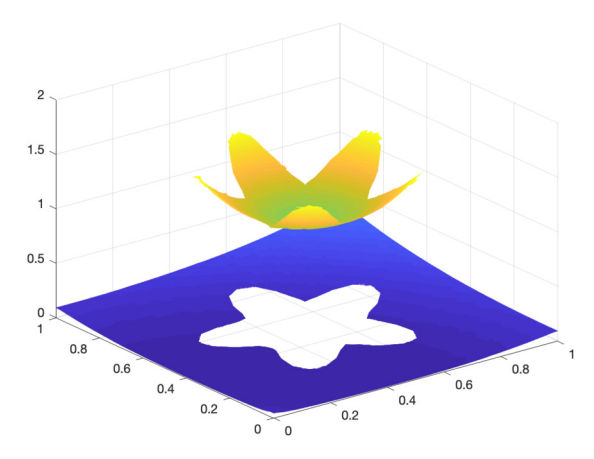


Fig. 8.10. Surface plot of the numerical solution u_h calculated by the PDWG method of Example 5.

Plotted in Fig. 8.9 are the interface and the domain (left), the computational interface at the first stage (middle), and the initial mesh (right). Fig. 8.10 shows the surface plot of the numerical solution u_h calculated by the PDWG method with k=1. Table 8.8 reports the approximation error and the corresponding rate of convergence for u_h and λ_h . An optimal order of convergence of $\mathcal{O}(h^k)$ for $\|u-u_h\|_0$ and $\|\lambda_h\|_w$ is observed, which is in good consistency with our theoretical findings in Theorem 7.2. Table 8.8 further suggests a convergence for $\|\lambda_0\|_1$ at the rate of $\mathcal{O}(h^{k+1})$, and a convergence for $\|\lambda_0\|_0$ at the rates of $\mathcal{O}(h^{k+1})$ and $\mathcal{O}(h^{k+2})$ for the linear and quadratic PDWG methods, respectively.

Example 6: We consider the problem (1.1)-(1.4) on the domain $\Omega=(0,1)^2$ with the same interface as that of Example 1; i.e., $\Omega_1=(0.25,0.75)^2$, $\Omega_2=\Omega\backslash\Omega_1$, and $\Gamma=\partial\Omega_1$. The coefficients are set as

$$a_1 = 2 + \sin(x + y)$$
, $a_2 = 5$, $\mathbf{b}_1 = \mathbf{b}_2 = (0, 0)$, $c_1 = c_2 = 0.4$.

Define

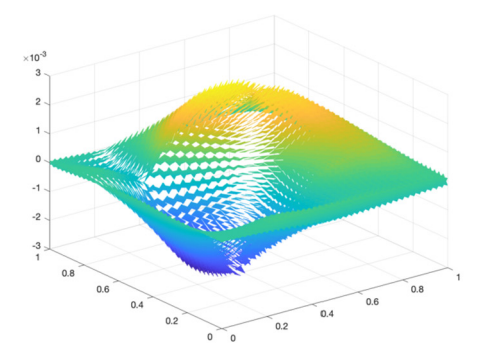
$$\Gamma_1 = \{ (\frac{1}{4}, y) : \frac{1}{4} \le y \le \frac{3}{4} \}, \quad \Gamma_2 = \{ (\frac{3}{4}, y) : \frac{1}{4} \le y \le \frac{3}{4} \},$$

$$\Gamma_3 = \{ (x, \frac{1}{4}) : \frac{1}{4} \le x \le \frac{3}{4} \}, \quad \Gamma_4 = \{ (x, \frac{3}{4}) : \frac{1}{4} \le x \le \frac{3}{4} \}.$$

LITOIS all	u converger	ice rates or	the mic	ii and quad	ratic 1 D	vva memou	3 IOI LAC	impic 5.	
	h	$\ \lambda_h\ _{\mathcal{W}}$	rate	$\ \lambda_0\ _1$	rate	$\ \lambda_0\ _0$	rate	$\ u-u_h\ _0$	rate
	3.82e-1	4.77e-2	-	1.20e-1	-	1.13e-2	_	7.18e-2	-
	1.91e-1	2.74e-2	0.80	5.66e-2	1.08	5.07e-3	1.16	3.35e-2	1.10
k = 1	9.53e-2	1.54e-2	0.83	1.70e-2	1.74	1.55e-3	1.71	2.01e-2	0.74
	4.77e-2	8.33e-3	0.89	4.85e-3	1.80	4.40e-4	1.81	9.26e-3	1.12
	2.38e-2	4.26e-3	0.97	1.27e-3	1.94	1.15e-4	1.94	4.77e-3	0.96
	h	$\ \lambda_h\ _{\mathcal{W}}$	rate	$\ \lambda_0\ _1$	rate	$\ \lambda_0\ _0$	rate	$ u-u_h _0$	rate
	3.82e-1	1.69e-2	-	7.29e-2	-	5.63e-3	_	1.12e-2	-
	1.91e-1	6.38e-3	1.41	2.47e-2	1.56	8.29e-4	2.76	2.97e-3	1.91
k = 2	9.53e-2	1.79e-3	1.83	3.73e-3	2.73	6.17e-5	3.75	8.28e-4	1.85
	4.77e-2	5.17e-4	1.80	5.17e-4	2.85	4.36e-6	3.82	2.33e-4	1.83
	2.38e-2	1.58e-4	1.71	6.91e-5	2.90	2.92e-7	3.90	5.42e-5	2.11

Table 8.8

Errors and convergence rates of the linear and quadratic PDWG methods for Example 5.



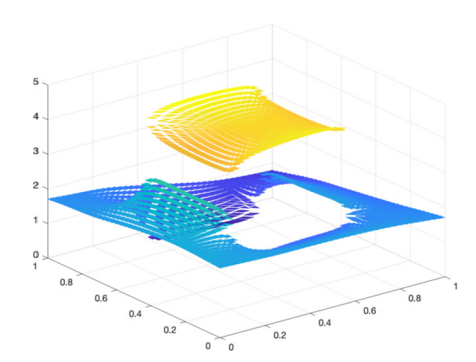


Fig. 8.11. Surface plot of the numerical solution λ_h (left) and u_h (right) calculated by the PDWG method of Example 6 with $f_1 = f_2 = 0, k = 1$ and h = 1/40.

We choose the boundary condition $u|_{\partial\Omega} = \frac{1}{5}\sin(x+y) + \cos(x+y) + 1$, and the following interface data:

$$[\![u]\!]_{\Gamma_i} = i, \quad 1 \le i \le 4, \quad [\![a\nabla u - \mathbf{b}u]\!]_{\Gamma_1} = (4,0), \quad [\![a\nabla u - \mathbf{b}u]\!]_{\Gamma_2} = (2/e^{\frac{3}{4}}e^x,0),$$

 $[\![a\nabla u - \mathbf{b}u]\!]_{\Gamma_3} = (0,6\pi\cos(2\pi y)), \quad [\![a\nabla u - \mathbf{b}u]\!]_{\Gamma_4} = (1,0).$

Fig. 8.11 shows the plots for the numerical solution λ_h (left) and u_h (right) obtained from the PDWG numerical method with k=1 for the interface problem when the right-hand side functions are taken as $f_1=f_2=0$. It should be noted that the exact solution to this interface problem is not known, and the interface data for the jump of u is piecewise constant and, therefore, does not have the $H^{\frac{1}{2}}(\Gamma)$ -regularity needed in most other numerical methods.

Example 7: This example assumes the same interface Γ as in Example 6. Here, we take

$$a_1 = 1$$
, $a_2 = 100$, $\mathbf{b}_1 = \mathbf{b}_2 = (2 + y, 1 + x)$, $c_1 = c_2 = 0$, $f_1 = f_2 = 0$.

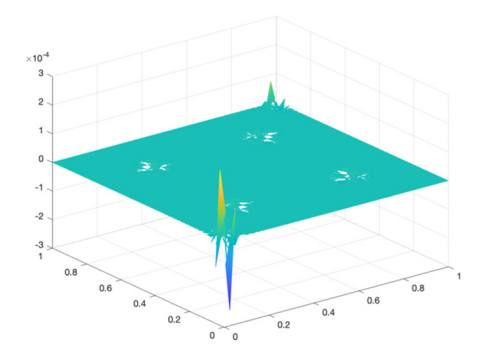
The boundary condition and the interface data are chosen as

$$\begin{split} u|_{\partial\Omega} &= \frac{1}{2}(x^2 + y^3)(\frac{1}{2}\sin(x + y) + \frac{1}{3}\cos(x + y)) - \frac{1}{3}\ln(x^2 + y^2), \\ & [\![u]\!]_{\Gamma_i} = 1, [\![u]\!]_{\Gamma_{i+2}} = 0, \ i = 1, 2, \\ & [\![a\nabla u - \mathbf{b}u]\!]_{\Gamma_1} = (\pi\cos(2\pi x), 0), \ [\![a\nabla u - \mathbf{b}u]\!]_{\Gamma_2} = (\frac{1}{2}\sin(x) + \frac{1}{4}\cos(x) + y, 0), \\ & [\![a\nabla u - \mathbf{b}u]\!]_{\Gamma_j} = ((y - \frac{1}{4})(y - \frac{3}{4})(\cos(x) + 2x), (\sin(x) + x^2)(2y - 1)), \ j = 3, 4. \end{split}$$

Fig. 8.12 shows the plots for the numerical solution λ_h (left) and u_h (right) obtained from the PDWG numerical method for the interface problem with k=2. For this test case, the exact solution to the interface problem is not known. Furthermore, the interface data for the jump of u is discontinuous by assuming 0 or 1 so that the $H^{\frac{1}{2}}(\Gamma)$ -regularity is not satisfied. The PDWG method, however, is applicable and provides meaningful numerical solutions.

CRediT authorship contribution statement

Chunmei Wang: propose the algorithm, develop the theory, and write the paper. Waixiang Cao: Numerical implementation and write the numerical test section. Junping Wang: Overview of the paper, discussion and suggestions for difficulties, and revise the paper.



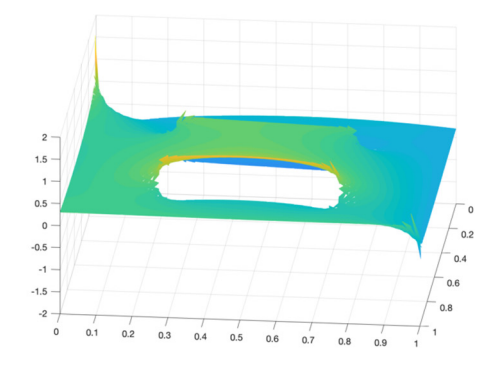


Fig. 8.12. Surface plot of the numerical solution λ_h (left) and u_h (right) calculated by the PDWG method of Example 7 with $f_1 = f_2 = 0$, k = 2 and h = 1/40.

Declaration of competing interest

The authors declare that they have no known competing financial interests or personal relationships that could have appeared to influence the work reported in this paper.

Data availability

No data was used for the research described in the article.

References

- [1] D. Bochkov, F. Gibou, Solving elliptic interface problems with jump conditions on Cartesian grids, arXiv:1905.08718.
- [2] J. Bedrossian, J.H. von Brecht, S.W. Zhu, E. Sifakis, J.M. Teran, A finite element method for interface problems in domains with smooth boundaries and interfaces, J. Comput. Phys. 229 (2010) 6405–6426.
- [3] P.A. Berthelsen, A decomposed immersed interface method for variable coefficient elliptic equations with non-smooth and discontinuous solutions, J. Comput. Phys. 197 (2004) 364–386.
- [4] J. Bramble, J. King, A finite element method for interface problems in domains with smooth boundaries and interfaces, Adv. Comput. Math. 6 (1996) 109–138.
- [5] E. Burman, M. Cicuttin, G. Delay, A. Ern, An unfitted hybrid high-order method with cell agglomeration for elliptic interface problems, hal-02280426v3, https://hal.archives-ouvertes.fr/hal-02280426v3, 2020.
- [6] E. Burman, P. Hansbo, Interior-penalty-stabilized Lagrange multiplier methods for the finite-element solution of elliptic interface problems, IMA J. Numer. Anal. 30 (2010) 870–885.
- [7] D. Chen, Z. Chen, C. Chen, W.H. Geng, G.W. Wei, MIBPB: a software package for electrostatic analysis, J. Comput. Chem. 32 (2011) 657-670.
- [8] T. Chen, J. Strain, Piecewise-polynomial discretization and Krylov-accelerated multigrid for elliptic interface problems, J. Comput. Phys. 16 (2008) 7503–7542.
- [9] Z. Chen, J. Zou, Finite element methods and their convergence for elliptic and parabolic interface problems, Numer. Math. 79 (1998) 175-2002.
- [10] I.-L. Chern, Y.-C. Shu, A coupling interface method for elliptic interface problems, J. Comput. Phys. 225 (2007) 2138-2174.
- [11] M. Dryjaa, J. Galvisb, M. Sarkisb, BDDC methods for discontinuous Galerkin discretization of elliptic problems, J. Complex. 23 (2007) 715-739.
- [12] R.E. Ewing, Z.L. Li, T. Lin, Y.P. Lin, The immersed finite volume element methods for the elliptic interface problems, Math. Comput. Simul. 50 (1999) 63–76.
- [13] R.P. Fedkiw, T. Aslam, B. Merriman, S. Osher, A non-oscillatory Eulerian approach to interfaces in multimaterial flows (the ghost fluid method), J. Comput. Phys. 152 (1999) 457–492.
- [14] W.H. Geng, S.N. Yu, G.W. Wei, Treatment of charge singularities in implicit solvent models, J. Chem. Phys. 127 (2007) 114106.
- [15] V. Girault, P. Raviart, Finite Element Methods for Navier-Stokes Equations, Theory and Algorithms, Springer-Verlag, Berlin, Heidelberg, New York, Tokyo, 1979.
- [16] R. Glowinski, T.-W. Pan, J. Periaux, A fictitious domain method for Dirichlet problem and applications, Comput. Methods Appl. Mech. Eng. 111 (1994) 283–303.
- [17] G. Guyomarc'h, C.O. Lee, K. Jeon, A discontinuous Galerkin method for elliptic interface problems with application to electroporation, Commun. Numer. Methods Eng. 25 (2009) 991–1008.
- [18] G.R. Hadley, High-accuracy finite-difference equations for dielectric waveguide analysis I: Uniform regions and dielectric interfaces, J. Lightwave Technol. 20 (2002) 1210–1218.
- [19] A. Hansbo, P. Hansbo, An unfitted finite element method, Comput. Methods Appl. Mech. Eng. 191 (2002) 5537–5552.
- [20] I. Harari, J. Dolbow, Analysis of an efficient finite element method for embedded interface problems, Comput. Mech. 46 (2010) 205–211.
- [21] X. He, T. Lin, Y. Lin, Interior penalty bilinear IFE discontinuous Galerkin methods for elliptic equations with discontinuous coefficient, J. Syst. Sci. Complex. 23 (2010) 467–483.
- [22] J.L. Hellrung Jr., L.M. Wang, E. Sifakis, J.M. Teran, A second order virtual node method for elliptic problems with interfaces and irregular domains in three dimensions, J. Comput. Phys. 231 (2012) 2015–2048.
- [23] J.S. Hesthaven, High-order accurate methods in time-domain computational electromagnetics. A review, Adv. Imaging Electron Phys. 127 (2003) 59-123.
- [24] T.P. Horikis, W.L. Kath, Modal analysis of circular bragg fibers with arbitrary index profiles, Opt. Lett. 31 (2006) 3417-3419.
- [25] S.M. Hou, X.-D. Liu, A numerical method for solving variable coefficient elliptic equation with interfaces, J. Comput. Phys. 202 (2005) 411-445.
- [26] S.M. Hou, W. Wang, L.Q. Wang, Numerical method for solving matrix coefficient elliptic equation with sharp-edged interfaces, J. Comput. Phys. 229 (2010) 7162–7179.
- [27] S.M. Hou, P. Song, L.Q. Wang, H.K. Zhao, A weak formulation for solving elliptic interface problems without body fitted grid, J. Comput. Phys. 249 (2013) 80–959.

- [28] T.Y. Hou, Z.L. Li, S. Osher, H.K. Zhao, A hybrid method for moving interface problems with application to the Hele-Shaw flow, J. Comput. Phys. 134 (2) (1997) 236–252.
- [29] L.N.T. Huynh, N.C. Nguyen, J. Peraire, B.C. Khoo, A high-order hybridizable discontinuous Galerkin method for elliptic interface problems, Int. J. Numer. Methods Eng. 93 (2013) 183–200.
- [30] A.T. Layton, Using integral equations and the immersed interface method to solve immersed boundary problems with stiff forces, Comput. Fluids 38 (2009) 266–272.
- [31] R.J. LeVeque, Z.L. Li, The immersed interface method for elliptic equations with discontinuous coefficients and singular sources, SIAM J. Numer. Anal. 31 (1994) 1019–1044
- [32] Z.L. Li, K. Ito, Maximum principle preserving schemes for interface problems with discontinuous coefficients, SIAM J. Sci. Comput. 23 (2001) 339-361.
- [33] Z.L. Li, K. Ito, The Immersed Interface Method Numerical Solutions of PDEs Involving Interfaces and Irregular Domains, Frontiers Appl. Math., SIAM, 2006.
- [34] J. Maryška, M. Rozlošník, M. Tuma, The potential fluid flow problem and the convergence rate of the minimal residual method, Numer. Linear Algebra Appl. 3 (1996) 525–542.
- [35] R. Massjung, An unfitted discontinuous Galerkin method applied to elliptic interface problems, SIAM J. Numer. Anal. 50 (2012) 3134-3162.
- [36] A. Mayo, The fast solution of Poisson's and the biharmonic equations on irregular regions, SIAM J. Numer. Anal. 21 (1984) 285-299.
- [37] L. Mu, J. Wang, G.W. Wei, X. Ye, S. Zhao, Weak Galerkin methods for second order elliptic interface problems, J. Comput. Phys. 250 (2013) 106-125.
- [38] L. Mu, J. Wang, X. Ye, S. Zhao, A new weak Galerkin finite element method for elliptic interface problems, J. Comput. Phys. 325 (2016) 157-173.
- [39] M. Oevermann, R. Klein, A Cartesian grid finite volume method for elliptic equations with variable coefficients and embedded interfaces, J. Comput. Phys. 219 (2006) 749–769.
- [40] C.S. Peskin, D.M. McQueen, A 3-dimensional computational method for blood-flow in the heart. 1. Immersedelastic fibers in a viscous incompressible fluid, J. Comput. Phys. 81 (1989) 372–405.
- [41] C.S. Peskin, Numerical analysis of blood flow in the heart, J. Comput. Phys. 25 (3) (1977) 220-252.
- [42] I. Ramiere, Convergence analysis of the q1-finite element method for elliptic problems with non-boundary-fitted meshes, Int. J. Numer. Methods Eng. 75 (2008) 1007–1052.
- [43] J. Wang, X. Ye, A weak Galerkin mixed finite element method for second-order elliptic problems, Math. Comput. 83 (2014) 2101–2126, arXiv:1202. 3655v2.
- [44] C. Wang, L. Zikatanov, Primal-dual weak Galerkin finite element methods for elliptic Cauchy problems, arXiv:1806.01583.
- [45] X.S. Wang, L.T. Zhang, L.W. Kam, On computational issues of immersed finite element methods, J. Comput. Phys. 228 (2009) 2535-2551.
- [46] A. Weigmann, K. Bube, The explicit-jump immersed interface method: finite difference methods for PDEs with piecewise smooth solutions, SIAM J. Numer. Anal. 37 (2000) 827–862.
- [47] K.N. Xia, M. Zhan, G.-W. Wei, MIB Galerkin method for elliptic interface problems, J. Comput. Appl. Math. 272 (2014) 195–220.
- [48] K.N. Xia, G.-W. Wei, A Galerkin formulation of the MIB method for three dimensional elliptic interface problems, Comput. Math. Appl. 68 (2014) 719–745
- [49] W.J. Ying, W.C. Wang, A kernel-free boundary integral method for implicitly defined surfaces, J. Comput. Phys. 252 (2013) 606-624.
- [50] S.N. Yu, G.W. Wei, Three-dimensional matched interface and boundary (MIB) method for treating geometric singularities, J. Comput. Phys. 227 (2007) 602–632
- [51] S.N. Yu, Y. Zhou, G.W. Wei, Matched interface and boundary (MIB) method for elliptic problems with sharp-edged interfaces, J. Comput. Phys. 224 (2) (2007) 729–756.
- [52] S.N. Yu, W.H. Geng, G.W. Wei, Treatment of geometric singularities in implicit solvent models, J. Chem. Phys. 126 (2007) 244108.
- [53] S. Zhao, High order matched interface and boundary methods for the Helmholtz equation in media with arbitrarily curved interfaces, J. Comput. Phys. 229 (2010) 3155–3170.
- [54] S. Zhao, G.W. Wei, High-order FDTD methods via derivative matching for Maxwell's equations with material interfaces, J. Comput. Phys. 200 (1) (2004) 60–103.
- [55] Y.C. Zhou, S. Zhao, M. Feig, G.W. Wei, High order matched interface and boundary method for elliptic equations with discontinuous coefficients and singular sources, J. Comput. Phys. 213 (1) (2006) 1–30.